NATIONAL HIGH MAGNETIC FIELD LABORATORY

REPORTS

VOLUME 11 • NO.1 • 2004

BIOLOGY

BIOCHEMISTRY

CHEMISTRY

CRYOGENICS

ENGINEERING MATERIALS

GEOCHEMISTRY

INSTRUMENTATION

KONDO/HEAVY FERMION SYSTEMS

MAGNET TECHNOLOGY

MAGNETIC RESONANCE TECHNIQUES

MAGNETISM AND MAGNETIC MATERIALS

METAL INSULATOR TRANSITIONS

MOLECULAR CONDUCTORS

OTHER CONDENSED MATTER

QUANTUM FLUIDS AND SOLIDS

SEMICONDUCTORS

SUPERCONDUCTIVITY - APPLIED

SUPERCONDUCTIVITY - BASIC

PREVIEWING THE 2003 NHMFL ANNUAL RESEARCH REVIEW

OPERATED BY: FLORIDA STATE UNIVERSITY • UNIVERSITY OF FLORIDA • LOS ALAMOS LABORATORY

NHMFL REPORTS

CONTENTS

Published by:
National High Magnetic Field Laboratory
1800 East Paul Dirac Drive
Tallahassee, Florida 32310-3706
Tel: 850 644-0311
Fax: 850 644-8350

Director: Jack Crow
Director of Government & Public Relations: Janet Patten
Editing and Writing: Kathy Hedick, Ceci Bell
Art Direction and Production: Walter Thorner

www.magnet.fsu.edu

This document is available in alternate formats upon request. Contact Ceci Bell for assistance. If you would like to be added to our mailing list please write us at the address shown at left, call 850 644-1933, or e-mail *bell@magnet.fsu.edu.*

from THE DIRECTOR'S DESK

Jack E. Crow

Announcing New Leaders of the Magnet Lab

It is with great pleasure that I announce that **Greg Boebinger has been chosen** to lead the NHMFL into the future. In early February, Greg accepted Florida State University's offer to become the **next director of the laboratory**, and immediately thereafter, Hugh Van Horn of the National Science Foundation described the selection as "a superb appointment." I couldn't agree more and truly believe that Greg is the best person to lead this world-class research facility, direct the renewal process, and drive ongoing efforts to expand facilities and enhance user services.

Greg's appointment was announced by Florida State University's Vice President for Research, Kirby Kemper. The transition in leadership will start in March when it is expected that Greg will be officially appointed at FSU and UF. Dr. Kemper, also a physicist, noted that the transition to a new director comes at a crucial time in the laboratory's development, as preparations for the lab's renewal proposal (due in December 2004) are already underway. "Greg's arrival is not only timely, but it's exciting, too. He's an extremely well known researcher in high magnetic fields and has demonstrated a tremendous talent for team leadership."

My long-time colleague and NHMFL principal investigator at the University of Florida, Neil Sullivan, shares this enthusiasm: "Greg has the insight and in-depth understanding of the impact of magnetic field research from physics to biology to the earth sciences. I am very excited about this appointment and look forward to building even stronger bridges between our institutions."

As most readers know, Greg joined the NHMFL in 1998 as director of the laboratory's Pulsed Field Facility at LANL. Last year, he was promoted to LANL Materials Science and Technology Deputy Division Leader for Science Programs, but continued to serve as the NHMFL principal investigator for operations at the Pulsed Field Facility. He began his training in physics as an undergraduate at Purdue University, where he holds degrees in electrical engineering and philosophy. He completed postgraduate work at Cambridge University in England before joining the doctorate program at MIT, where he received the Ph.D. in physics in 1986. Prior to moving to Los Alamos, Greg was a staff physicist at Bell Laboratories, specializing in high field pulsed magnets.

On January 28, following a six-month international search, Paul Follansbee, LANL MST Division Leader, announced the selection of **Alex Lacerda as the new director of the NHMFL Pulsed Field Facility**. The search was led by LANL and the committee included representatives from all three sites of the NHMFL and the user community. I strongly endorse Alex's promotion and am confident in his ability to lead NHMFL operations at LANL to new levels. Dr. Follansbee's announcement:

It is a pleasure for me to announce that Alex Lacerda has been named the Center Leader for the National High Magnetic Field Laboratory.

Alex has a long history of contributions to LANL's campus of the NHMFL, starting with a Visiting Scientist assignment in 1991 – 1992. He spent three years as an Assistant Scholar at Florida State University, site of the 2nd (and largest) campus of NHMFL, and he is an Adjunct Professor at Florida State University and at the University of Florida (3rd campus of NHMFL). He joined the Laboratory in 1996. Alex received his Ph.D. from the University of Joseph Fourier, Grenoble. He has published extensively in areas related to use of magnetic fields in characterization of materials and developing an understanding of the underlying condensed matter physics.

Alex has served as Acting Center Leader of the NHMFL since May, 2003. During this time he has continued to strengthen the external user program within NHMFL, broaden the scope of this group within MST Division, and increase interactions across the Laboratory. In particular, Alex has become an advocate for the sharing of best practices among the Laboratory Centers and for an increased contribution of the Laboratory Centers in Laboratory mission areas.

Alex will now assume a permanent position on the NHMFL Executive Committee with UF and FSU. I welcome the opportunity for Alex to become a permanent member of the MST Division Leadership Council. Please join me in congratulating Alex.

In conclusion, I wholehearted support both of these promotions and look forward to working with Greg and Alex through the transitions. The foundation of the laboratory's world stature and pre-eminence rests on the dedication, commitment, knowledge, and skills of its faculty and staff. It has been, and continues to be, my honor to be a part of the group. My farewells will come another day. Today, I extend my sincerest congratulations to my friends and colleagues, Greg Boebinger and Alex Lacerda.

Best regards,

Jack Crow

Greg Boebinger

Alex Lacerda

FROM THE CHIEF SCIENTIST'S DESK

J. Robert Schrieffer

Previewing the 2003 NHMFL Annual Research Review

As in the past years, the science program of the NHMFL continued to grow in strength and size in 2003. There was strong collaborative research by users and in-house scientists ensuring broad benefit to the scientific community of the unique facilities of the laboratory. This year 372 research reports were submitted in 18 areas of research as compared to 380 reports in 2002. Reports sponsored by the NHMFL In-House Research Program are denoted by **[IHRP]** in the text.

The number of reports in each of the categories is as follows: biochemistry 44, biology 27, chemistry 27, cryogenics 6, engineering materials 12, geochemistry 12, instrumentation 10, kondo/heavy fermions 24, magnet technology 4, magnetic resonance techniques 32, magnetism and magnetic materials 50, metal-insulator transitions 6, molecular conductors 23, other condensed matter 19, quantum fluids and solids 6, semiconductors 30, superconductivity applied 13, and superconductivity basic 27.

In order to give a flavor of the overall research program we are pleased to feature here one report from each category. In the case of Geochemistry, Magnetism and Magnetic Materials, and Molecular Conductors, two reports are presented. The task of determining which reports to highlight was extremely difficult, as many other research efforts are of comparable strength.

CATEGORY	*2000*	*2001*	*2002*	*2003*	*TOTAL*
BIOLOGY	47	49	54	27	177
BIOCHEMISTRY				44	44
CHEMISTRY	27	31	39	27	124
CRYOGENICS	5	5	3	6	19
ENGINEERING MATERIALS	6	5	10	12	33
GEOCHEMISTRY	13	10	13	12	48
INSTRUMENTATION	16	10	9	10	45
KONDO/HEAVY FERMION SYSTEMS	19	21	26	24	90
MAGNET TECHNOLOGY	6	7	17	4	34
MAGNETIC RESONANCE TECHNIQUES	19	24	24	32	99
MAGNETISM AND MAGNETIC MATERIALS	36	45	48	50	179
METAL-INSULATOR TRANSITIONS				6	6
MOLECULAR CONDUCTORS	19	24	27	23	93
OTHER CONDENSED MATTER	10	13	15	19	57
QUANTUM FLUIDS AND SOLIDS	3	6	4	6	19
SEMICONDUCTORS	27	32	38	30	127
SUPERCONDUCTIVITY - APPLIED	16	11	32	13	72
SUPERCONDUCTIVITY - BASIC	26	29	21	27	103
	295	*322*	*380*	*372*	*1369*

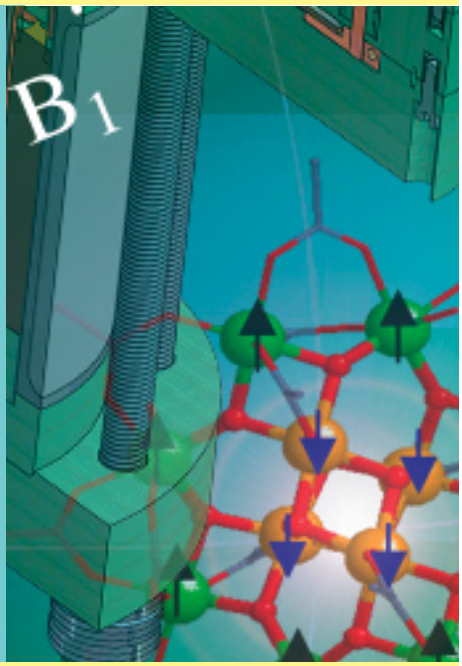

BIOCHEMISTRY

Structural Analysis of 2D-Gel-Separated Glycoproteins from Human Cerebrospinal Fluid by Tandem High Resolution Mass Spectrometry

Håkansson, K., NHMFL
Emmett, M.R., NHMFL/FSU, Chemistry and Biochemistry
Marshall, A.G., NHMFL/FSU, Chemistry and Biochemistry
Davidsson, P., Göteborg Univ., Institute of Clinical Neuroscience (Sweden)
Nilsson, C.L., Göteborg Univ., Institute of Medical Biochemistry (Sweden)

The feasibility of global glycoprotein analysis by electrospray ionization Fourier transform ion cyclotron resonance mass spectrometry and infrared multiphoton dissociation (IRMPD) tandem mass spectrometry is demonstrated. Combined 2D gel glycoprotein separation and visualization, in-gel digestion and accurate (<10 ppm) mass measurement allowed identification of human glycoproteins and revealed differences in glycosylation. IRMPD obviates the need for glycan release, which prevents sample dispersal, and allows the assignment of glycan structures to specific sites of N-glycosylation.

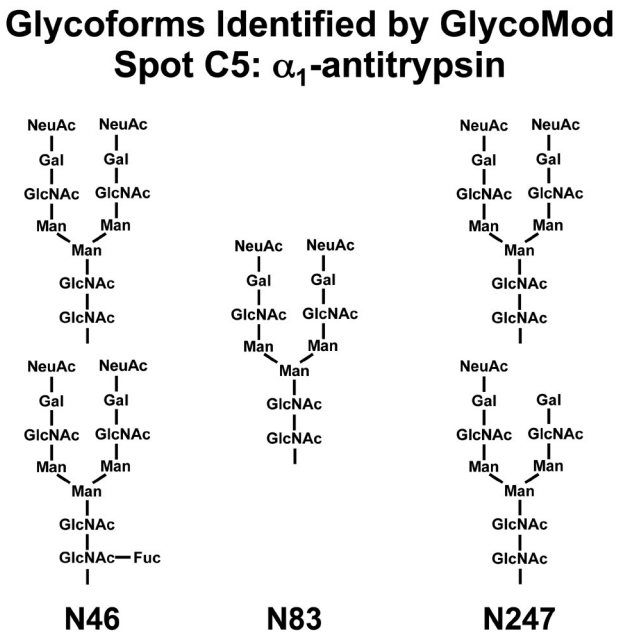

Figure 1. Glycan structures determined for asparagines 46, 83, and 247 of α_1-antitrypsin glycopeptides from gel spot C5.

Acknowledgements: This work was supported by Vetenskapsrådet, the NSF National High-Field FT-ICR User Facility (CHE 99-09502), Florida State University, the National High Magnetic Field Laboratory in Tallahassee, FL, the Swedish Foundation for International Cooperation in Research and Higher Education (STINT), Fredrik och Ingrid Thurings Stiftelse, and Stiftelsen Syskonen Svenssons Fond. We thank Michael J. Chalmers, Christopher L. Hendrickson, John P. Quinn, and Bruce E. Wilcox for instrumentation development and fruitful discussions that made this work possible.

[1] Håkansson, K., *et al*., *J. Proteome Res.*, **2**, 581-588 (2003).

BIOLOGY

Noninvasive Monitoring of Stem Cell Delivery and Muscle Regeneration

Frimel, T.N., Malcom Randall Veterans Administration Medical Center; UF, Physical Therapy
Cahill, K.S., UF, Molecular Genetics and Microbiology
Gaidosh, G.S., UF, Physiology and Functional Genomics
Torres, R.T., UF, Advanced Magnetic Resonance Imaging and Spectroscopy Facility/NHMFL
Huard, J., Univ. of Pittsburgh, Orthopedic Surgery
Byrne, B.J., UF, Pediatrics
Vandenborne, K., UF, Physical Therapy
Walter, G.A., UF, Physiology and Functional Genomics

Introduction: Cast immobilization causes skeletal muscle disuse atrophy and an increased susceptibility to muscle damage. The underlying muscle atrophy occurs due to apoptosis and the silencing of endogenous muscle stem cells,[1] whereas, subsequent reambulation promotes extensive muscle regeneration through the recruitment of muscle stem cells.[2] Stem cell transfer for enhanced muscle regeneration has tremendous therapeutic potential especially in the muscular dystrophies and during sarcopeana. Previous analysis of stem cell delivery has relied on traditional invasive techniques to monitor the effectiveness of delivery. The purpose of this study was to evaluate the ability of MR imaging to noninvasively monitor muscle stem cell transplantation, homing to damaged tissue, and regeneration.

Methods: Ten female C57BL6 mice underwent hindlimb immobilization for 2 weeks using a bilateral casting procedure that produces a well defined model of soleus muscle damage and regeneration during reloading.[3] Multipotent muscle derived stem

cells ($0.5x10^6$) constituently expressing a histological marker gene (β-galactosidase) were delivered either via direct intra-muscular injection into the mouse hindlimb or arterial injection into the abdominal aorta following 48 hours of muscle reloading. At this time point, muscle damage and T_2 contrast in the reambulated mouse soleus is maximal.[3] Unilateral occlusion of the iliac artery ensured that the arterial injected cells were delivered to one hindlimb. Muscle stem cells were labeled with a supraparamagnetic iron-oxide contrast agent (ferumoxide-poly-l-lysine) to allow for the detection of stem cell transfer using T_2 and T_2* weighted MR images.[4] MR measurements were performed on a 4.7 Tesla Bruker Avance Imaging Spectrometer with a single tuned 1.6 cm solenoid coil immediately post-injection and at 1, 3, and 7 days post-injection. T_2 weighted images were acquired immediately post injection and at 3 days post injection using a spin echo sequence (TE=14, 40ms, TR=2000ms, FOV=1.6cm, 256x128, 2nex, thk=1.0mm) and T_1 weighted images were acquired using a 3D gradient echo sequence (TE=4.5,7ms, TR=17ms). T_2 maps were created by using the decay in pixel signal intensity as a function of TE on the spin-echo sequences. T_2 was used as an indicator of muscle damage. Cells were visualized on all scans as the absence of signal. Histological analyses (Hematoxylin & Eosin; X-gal; Prussian Blue) were performed to confirm muscle damage and stem cell incorporation.

Results: Reambulation following cast immobilization induced specific muscle damage to the soleus, an important postural muscle. Examination of the MR images acquired during reambulation showed an increase in T_2 in the soleus muscle consistent with muscle damage (see Fig. 1B and 1D). Regions of increased T_2 in the soleus muscle on MR scans were confirmed using hematoxylin and eosin stains. As previously reported muscle derived stem cells were efficiently labeled *in vitro* by transfection with ferumoxide-poly-L-lysine complexes.[4] Labeled stem cells underwent normal myogenesis *in vitro* and *in vivo*. Transplantation of labeled stem cells resulted in regions of hypo-intensity on T_1, T_2, and T_2* weighted MR scans. Following the direct intra-muscular injection of labeled stem cells, regions of hypo-intensity could be detected in the regenerating soleus musculature as well as other posterior hindlimb muscles (Fig.1B). Engrafted cells were detected by analysis of β-galactosidase (LacZ) activity, and iron content. LacZ expressing fibers were identified in regions corresponding to the MR images (Fig.1A). Additionally, Prussian blue staining of the corresponding serial section revealed the presence of iron accumulation in the LacZ positive fibers. However, a small number of non-muscle cells contained iron. Due to the number of macrophages seen in regenerating muscle fibers, we hypothesize these to be scavenger cells removing the remains of labeled cells that fail to engraft. Additionally, MRI allowed for the non-invasive analysis of mc13 cell engraftment following arterial delivery. Small, punctuate areas of decreased signal intensity were seen in the musculature of the leg that received the labeled cell infusion (Fig. 1D). The contra-lateral limb and control limbs injected with unlabeled cells did not contain these characteristic areas. Histological analyses of the leg musculature revealed cells within the vasculature distributed in patterns corresponding to the

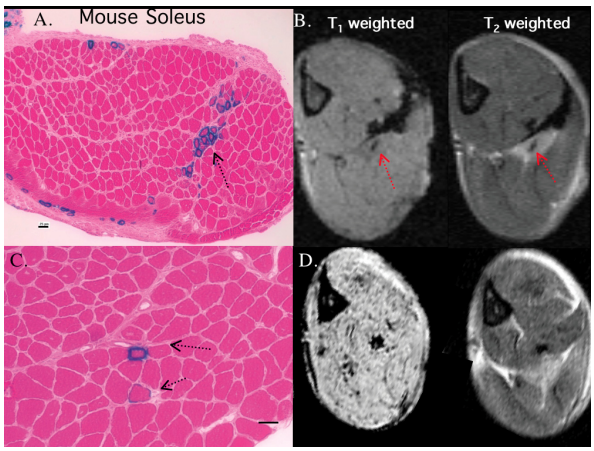

Figure 1. Targeting of muscle derived stem cells to the mouse soleus following casting and reambulation. Note the hyperintense regions due to muscle damage on T2 weighted images, and the hypointense regions corresponding to cell deposition on both T1 and T2 weighted images.

MR images. Importantly, in direct contrast to the local injection of labeled cells, label from non-engrafted cells was efficiently and rapidly cleared from the musculature. Following arterial delivery of c2c12 cells, a cell type that results in extremely low engraftment rates, labeled cells were removed by 3 days post injection. Following the arterial delivery of mc13 cells to the hindlimbs, the majority of cells remained trapped in the capillary lumens for up to 2 weeks post-injection. X-gal staining confirmed the presence of stem cell integration in the soleus following vascular delivery (Fig. 1C).

Conclusion: MRI can be utilized to monitor not only muscle damage and regeneration following hindlimb immobilization but also therapeutic muscle stem cell transfer. Although the rate of stem cell incorporation was significantly lower following vascular delivery compared to the direct intra-muscular injection, stem cell derived myotubes could still be identified in the regenerating soleus.

[1] Allen, D.L., *et al*., *Muscle Nerve*, **10**, 1350-60 (1999).
[2] Hawke, T.J., *et al*., *J. Appl. Physiol*., **91**, 534-551 (2001).
[3] Frimel, T.N., *et al*., "Muscle damage and regeneration following cast-immobilization using T_2 weighted magnetic resonance imaging," ISMRM, Toronto, Canada, 2003.
[4] Cahill, K.S., *et al*., "Noninvasive monitoring and tracking of muscle stem cells," ISMRM, Toronto, Canada, 2003.

CHEMISTRY

High Resolution ^{7}Li Solid State NMR Study of $Li_xV_2O_5$ Cathode Electrodes for Li-Rechargeable Batteries

Fu, R., NHMFL
Ma, Z., NHMFL
Zheng, J.P., FAMU-FSU College of Engineering
Au, G., U.S. Army Communications-Electronics Command
Plichta, E.J., U.S. Army Communications-Electronics Command
Ye, C., Wuhan Institute of Physics and Mathematics, Chinese Academy of Sciences

The $Li_xV_2O_5$ cathode of Li-rechargeable battery cells under three different charge states have been studied by high-resolution solid-state ^{7}Li magic angle spinning (MAS) NMR spectroscopy. In the charged and discharged states, three different ^{7}Li NMR resonances, corresponding to the Li^+ ions in the electrolyte, in the V_2O_5 cathode, and on the surface of the V_2O_5 cathode, were identified by their spin-lattice relaxation times in inversion recovery experiments, as shown in Fig. 1. Only signals of the Li^+ ions in the electrolyte were observed in the over charged state. It is shown experimentally that the Li^+ ions in the electrolyte experience a dynamics or exchange process on a timescale of milliseconds with those in the V_2O_5 cathode, in particular for the discharged state, where a severe cross relaxation effect was observed in the inversion recovery for the Li^+ ions in the electrolyte, as shown in Fig. 2. It is concluded that such an exchange is mediated by the Li^+ ions on the surface of the V_2O_5 cathode. Therefore, the surface structure of the V_2O_5 cathode electrode plays an important role in the reversibility of the Li^+ ions in the rechargeable battery.

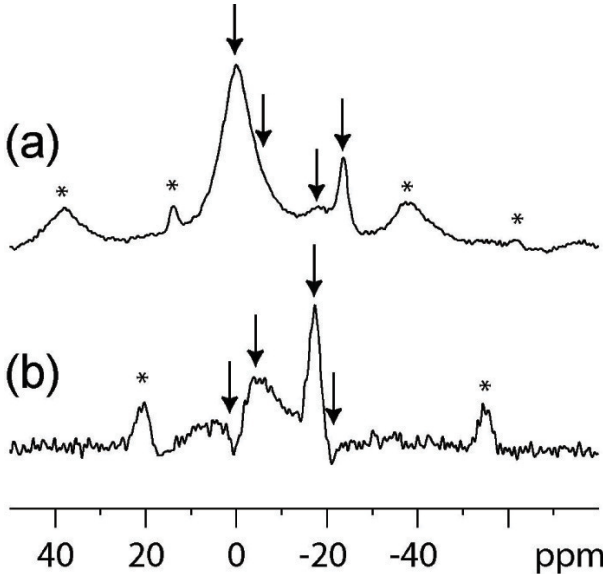

Figure 1. ^{7}Li MAS NMR absorption spectra of the $Li_xV_2O_5$ cathode materials at different inversion recovery times. (a) The recovery time was 230 ms for the discharged state. (b) The recovery time was set to 18 ms for the charged state. The asterisks indicate the spinning sidebands while the arrows represent the positions of the isotropic chemical shifts.

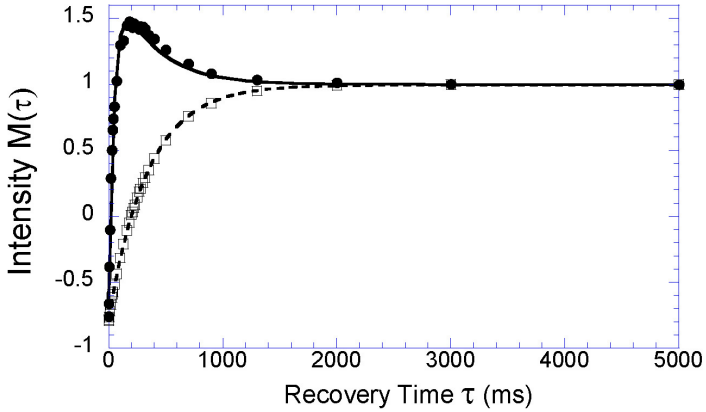

Figure 2. Plot of ^{7}Li signal intensities M(τ) of the $Li_xV_2O_5$ cathode as a function of recovery time τ at the discharged state. All of the experimental data were recorded on a Bruker DMX600 NMR spectrometer at 300 K and normalized to their equilibrium magnetizations. The solid circles and the squares indicate the signal intensities integrated from -8 to +8 ppm and from -15 ppm to -30 ppm, corresponding to the chemical shifts of the Li^+ ions in the electrolyte and in the cathode, respectively.

Acknowledgements: This work is partially supported by the U.S. Army Communications-Electronics Command.

CRYOGENICS

Measurement of He II Thermal Counterflow Using PIV Technique

Zhang T., NHMFL/FAMU-FSU College of Engineering
Van Sciver, S.W., NHMFL/FAMU-FSU College of Engineering

Thermal counterflow is a unique fluid-dynamic feature of He II due to the existence of two fluid components, normal fluid and superfluid. An in-depth investigation of thermal counterflow

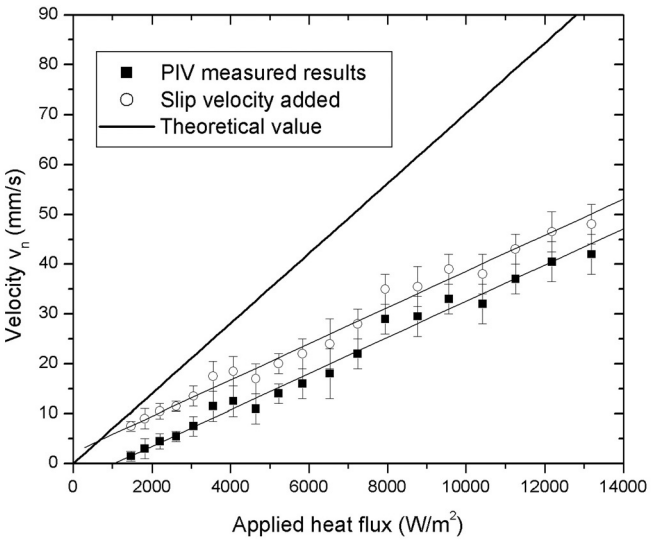

Figure 1. PIV measured particle velocity and theoretical normal-fluid velocity versus heat flux at 1.80 K.

requires the measurement of its global velocity field, which can be achieved using the Particle Image Velocimetry (PIV) technique. To successfully apply PIV to He II, one has to select the appropriate tracer particles, and properly seed them into liquid helium. In this study, polymer particles from Bangs Laboratory® were selected because of their extremely small particle size (~ 1.7 μm). From the particle dynamics in He II, they have a slip velocity around 1 mm/s and a relaxation time around 0.1 ms. Also, a new seeding method using two-phase fluidized bed technique was developed, giving the ability to generate an adequate particle concentration with reduced particle aggregation.

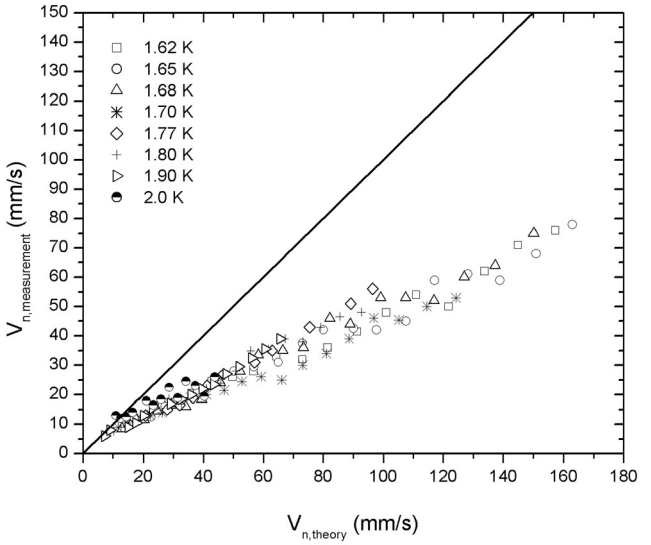

Figure 2. Comparisons between PIV-measured velocities and theoretical normal-fluid velocities at different temperatures (the solid line represents where $v_{n,measurement} = v_{n,theory}$).

The PIV measurement of thermal counterflow was conducted inside a specially designed optical cryostat. The counterflow channel was made of 6.5 mm thick G-10 plate with a 43 × 19.5 mm^2 cross-section area. Fig. 1 shows that there exists an apparent discrepancy between the PIV measured particle velocity and the theoretical normal fluid velocity, which was assumed at first to result from the slip velocity between tracer particles and liquid helium. The discrepancy still exists, however, with the slip velocity added to the PIV measurement results, indicating that slip velocity is not the primary cause for the discrepancy. In their counterflow jet experiment, Nakano and Murakami[1] suggested that the discrepancy can be explained by the relation, $v_{n,measurement} = \frac{\rho_n}{\rho} v_{n,theory}$, which means the ratio of measured normal-fluid velocity to its theoretical value is equal to the ratio of normal-fluid density to the bulk density of He II. This relation indicates a strong temperature dependence of the ratio $\frac{v_{n,measurement}}{v_{n,theory}}$. However, our results show that the ratio is most likely temperature independent and constant at around 0.45 (see Fig. 2). It is still unclear what exactly causes the discrepancy between the particle and theoretical normal-fluid velocities. However, previous research from Donnelly *et al*.[2] and Chung and Critchlow[3] give us the hint that the superfluid component in He II, even though it is inviscid, may exert an additional force on the tracer particles. This force, which is in opposite direction to the viscous drag force from the normal-fluid component, would prevent the tracer particles from tracking the normal-fluid velocity, and thus cause the velocity discrepancy.

Acknowledgements: This work is supported by the National Science Foundation – Chemical Transport Systems Division under grant number CTS-0001411.

[1] Nakano, A., *et al*., *Cryogenics*, **34**, 179-185 (1994).
[2] Donnelly, R.J., *et al*., *J. Low Temp. Phys*., **126**, 327-332 (2002).
[3] Chung, D.Y., *et al*., *Phys. Rev. Lett*., **14**, 892-894 (1965).

ENGINEERING MATERIALS

Role of Nanotwins and Dislocations in High Strength and High Conductivity Bulk Cu [IHRP]

Han, K., NHMFL
Ishmaku, A., NHMFL
Embury, J.D., MacMaster Univ., Materials Science and Engineering, Hamilton (Canada)

Strength and conductivity are among the most important parameters for high field magnet conductors. The development of such conductors requires fundamental research into the influence

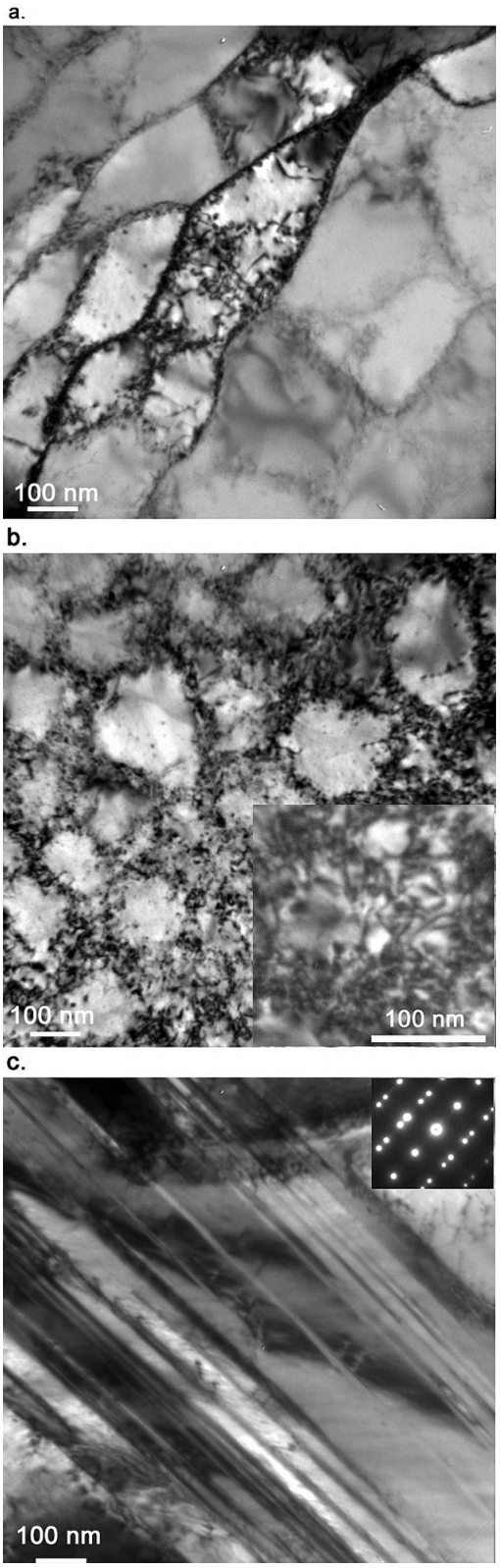

Figure 1. Comparison of the transmission-electron-microscopy images from samples deformed at room temperature (a) and at liquid-nitrogen temperature (b) and (c). The deformation strain was 2.5 and the thin foils were sectioned perpendicular to the drawing direction in the center of the wires.

of various defects on the resistivity and strength of conductive materials.

Resistance in metallic materials can be represented by a form of Mathiessen's law as follows:

$$\rho = \rho_t + \rho_I + \rho_b + \rho_d , \quad (1)$$

in which ρ_t, ρ_I, ρ_b and ρ_d represent the thermal, impurity, interface and defect contributions, respectively. The development of high-strength materials often involves the addition of various alloy elements to form either multiphases, or solid solution, and therefore increases ρ_t, ρ_I or ρ_b or combination of them. Therefore, achievement of both high strength and high conductivity in a multi-functional, bulk material is challenging, since the majority of the strengthening components reduce the conductivity of the materials significantly. Because dislocations have little scattering effect on conduction electrons, a high density of dislocations can strengthen conductors without significantly increasing the resistivity. Room-temperature (RT) deformation (RT defined as 295 ± 2 K in this report), however, can only store a limited number of dislocations in pure metals due to dislocation annihilation, i.e. recovery. This limitation is expanded by a well controlled, liquid-nitrogen-temperature (LNT) deformation process (LNT defined at 77 ± 0.5 K in this report), which, as shown in Fig. 1, permits accumulation of both nano-twins and a high density of refined dislocation cells accompanied by much lower degree of recovery than RT deformation. This results in a bulk pure Cu with yield strength about nine times that of annealed pure Cu. The hardness data show that the center areas of rods processed in this way have lower hardness than the area adjacent to the surface. Therefore, overall strengths should be even higher because our data represent sections from the center areas of drawn wires.

The resistivity changes, $\Delta\rho_d$ and $\Delta\rho_b$, resulting from defects accumulated at cryogenic temperatures can be subdivided into two portions. The first portion is $\Delta\rho_{d\text{-}ret}$ plus $\Delta\rho_{b\text{-}ret}$ resulting from retainable defects (*d-ret*). Those defects, with defect density of $\Delta\delta_{d\text{-}ret}$ and $\Delta\delta_{b\text{-}ret}$, contribute to the strain hardening and resistance increase, and remain in the crystal after the materials are warmed to RT. The second portion can be thought of as vacancy dipoles, which may move by short-circuit diffusion and could be removed between 77 K and 300 K. This portion of the defects results in a change of resistivity by an amount of $\Delta\rho_{d\text{-}rec}$. Our *in situ* measurement demonstrated $\Delta\rho_{d\text{-}rec}/\rho$ is about 10% at 77 K after materials were LNT-deformed by $\varepsilon_d = 0.05$ and then warmed to RT. Because of the occurrence of both dynamic and static recoveries at low temperatures, the lower the deformation temperature, the higher the $\Delta\delta_{d\text{-}ret}$, the $\Delta\delta_{b\text{-}ret}$, the ρ, and the yield strength. The *in situ* measurement of the resistance of the LNT-deformed samples warmed from 77 K to RT showed no abrupt changes of the resistance with respect to the temperatures. Therefore, annihilation of the dislocations and defects accumulated by cryogenic deformation of Cu occurred gradually rather that at a defined temperature.

In summary, the LNT deformation process provides a simple and economic approach to the production of high-strength, low-resistance, bulk Cu by introducing both nanotwins and refined dislocation cell structures.

Determination of Neodymium – Fulvic Acid Binding Constants by Capillary Electrophoresis Inductively Coupled Plasma Mass Spectrometry (CE-ICP-MS)

Sonke, J., NHMFL
Salters, V.J.M., NHMFL/FSU, Geological Sciences

Capillary Electrophoresis Inductively Coupled Plasma Mass Spectrometry (CE-ICP-MS) has been used to study Neodymium – Suwannee River Fulvic Acid (FA) interaction at pH 6-9 and 0.001 - 0.1 mol.L^{-1} ionic strength. The use of a strong ligand (EDTA) competition method allowed us to successfully manipulate a bimodal species distribution of Nd.FA and NdEDTA. These two species have sufficiently different charge and shape characteristics to be easily separable by CE, even in the presence of nebulizer induced siphoning. Due to strong metal-ligand complex stability for both Nd.FA and Nd.EDTA, quantitative bias due to complex dissociation was found to be negligible; a method development scheme for quantitative CE-ICP-MS addresses metal-ligand dissociation specifically and is outlined in this study. Siphoning induced laminar flow was optimized and used as an advantage to speed up separations and can play an important role in avoiding quantitative speciation bias. Log values of conditional binding constants for Nd-FA complexation at 0.1 mol.L^{-1} ionic strength varied gradually from 9.1 to 12.5 over the pH range 6-9. Detection limits for Nd speciation were 500 pM.

Rare Earth Element – Humic Acid Interaction: Experimental Evidence for Kinetic and Equilibrium Fractionation in Aqueous Systems

Sonke, J.E., NHMFL
Salters, V.J.M., NHMFL/FSU, Geological Sciences
Benedetti, M.F., Univ. Pierre et Marie Curie, Laboratoire Géochimie & Métallogenie Paris (France)

Dissolved organic matter (DOM) is well known for its strong binding capacity for trace metals. In order to better predict the role of DOM in the speciation and transport of trace metals in the environment we coupled capillary electrophoresis (CE), a molecular separation technique, to a Sector Field Inductively Coupled Plasma Mass Spectrometer (SF-ICP-MS). The combination of these two techniques allows for the study of non-labile metal speciation in aquatic samples.

By separating Rare Earth Element (REE) complexes with EDTA and Humic Acids (i.e. ligand competition), we have been able to determine conditional equilibrium binding constants (K_c) and kinetic rate constants for all 14 REEs with Humic (HA) and Fulvic Acids (FA) as a function of pH (6-9) and ionic strength (IS, 0.01-0.1 mol/L). Assuming a 1:1 binding mechanism, $\log K_c$ values for REE-FA varied from 9.0 (La) to 10.5 (Lu) at pH 6, 0.1 mol/L IS, and 11.7 (La) to 14.6 (Lu) at pH 9, 0.1 mol/L IS. $\log K_c$ values for REE-HA were 10.6 (La) to 12.2 (Lu) at pH 6, 0.1 mol/L IS and 13.2 (La) to 16.5 (Lu) at pH 9, 0.1 mol/L IS. Slightly higher values for K_c were obtained at 0.01 mol/L IS. The general observations of stronger REE-HA binding compared to REE-FA, and stronger binding with increasing pH and decreasing IS correlate with our current understanding of metal-DOM interactions.[1] Both K_cs as well as kinetic rate constants increase with increasing REE mass number (decreasing ionic radius); a reflection of the well-known lanthanide contraction.

This is the first comprehensive metal binding dataset between REE and DOM, and the first experimental evidence for differential equilibrium and kinetic binding behavior between REEs and DOM. The 30-1000 fold increase in binding strength of heavy REEs with DOM provides for an equilibrium fractionation mechanism that may explain features of the global geochemical REE cycle such as fractionation related to weathering, estuarine mixing, and REE scavenging in the deep ocean.[2] The experimental dataset has also been interpreted with the Non-Ideal Competitive Adsorption – Donnan (NICA-Donnan[1] model for HA and FA metal binding, such that REE-HA binding can be predicted as a function of pH and IS. The NICA-Donnan model is a standard object in the novel object oriented chemical speciation code ORCHESTRA (Objects Representing Chemical Speciation and Transport)[3] that we used to explore the possible effects of pH and IS on fractionating the REEs along an estuarine gradient.

---

1 Milne, C.J., *et al*., *Environmental Science & Technology*, **37**, 958-971 (2003).
2 Elderfield, H., *et al*., *Geochimica Et Cosmochimica Acta*, **54**, 971-991 (1990).
3 Meeussen, J.C.L., *Environmental Science & Technology,* **37**, 1175-1182 (2003).

A Method to Study Angle-Dependent High Field Microwave Magneto-Conductivity Using a Cavity Perturbation Technique

Takahashi, S., UF, Physics
Hill, S., UF, Physics/NHMFL

The cavity perturbation technique is an extremely powerful method to study high field microwave magneto-conductivity of conducting samples,[1] as well as high-frequency electron paramagnetic resonance (EPR).[2] However, it also poses complications if one wishes to study angle-dependent effects in anisotropic single crystal samples within the limited space of an axial high field magnet. We have recently developed compact rotating cylindrical cavities that overcome these problems. The cylinder is mounted transverse to the bore of the axial high field magnet, coupling is achieved through the side walls of the cavity, and the end plate is then rotated by means of an external drive instead of the body of the cavity itself (see schematic in Fig. 1). Therefore, the rotation does not affect the cylindrical geometry of the cavity, or the mechanical connections to the waveguides. The TE011 mode frequency of the loaded cavity is 52 GHz, with the possibility to work on higher-order modes to frequencies well above 100 GHz. Neither the quality factor (~18,000 for the fundamental mode) nor coupling to the cavity are affected by full 360° rotation. Use of higher-order modes allows wide frequency coverage (45 to 200 GHz). The rotation mechanism provides reasonable accuracy (0.18° resolution), and is compact enough to enable measurements in the high field resistive and Hybrid magnets at Tallahassee. A photograph of the cavity is shown in Fig. 2.

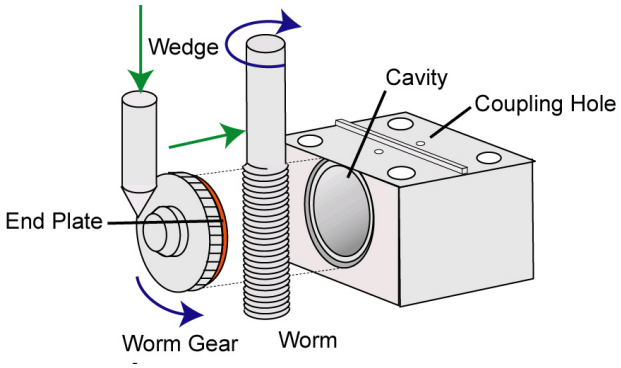

Figure 1. Schematic of the rotating cavity design. The worm gear that controls the rotation of the cavity end-plate may be operated from outside the cryostat. A second drive ensures good contact between the end-plate and the main body of the cavity during measurements; this drive also releases the end-plate for rotation.

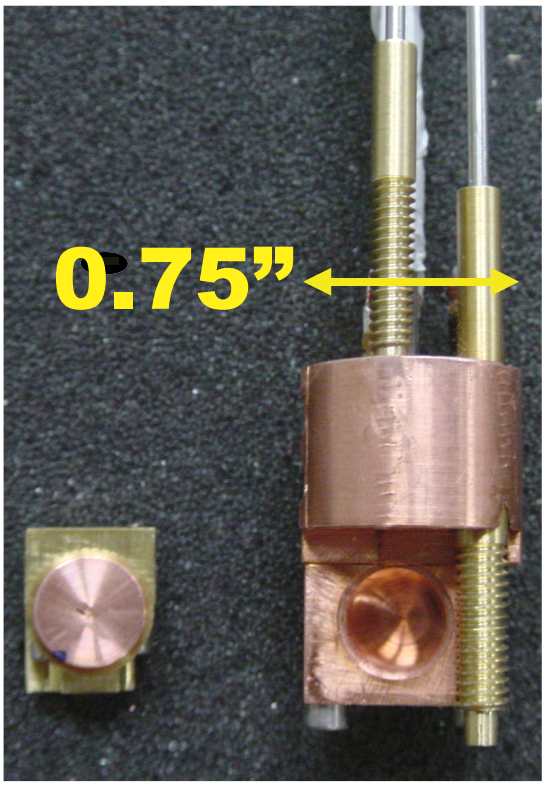

Figure 2. Photograph of the cavity assembly.

We have tested two versions of the rotating cavity: a prototype was tested in the wide-bore 25 T magnets; subsequently, miniaturization allowed for experiments in the narrow bore 33 T magnets. To date, these cavities have been used for a range of different studies, including: angle dependent single crystal EPR measurements on the Mn_{12}-ac single molecule magnet system; and a novel form of cyclotron resonance in a series of anisotropic organic conductors. Several of these experiments are reported elsewhere in this annual report.

Acknowledgements: This work was supported by NSF (DMR0239481 and DMR0196430) and Research Corporation.

[1] Kovalev, A.E., *et al*., *Phys. Rev. Lett*., **91**, 216402 (2003).
[2] Hill, S., *et al*., *Phys. Rev. Lett*., **90**, 217204 (2003).

Possible Magnetic-Field-Induced Structural Phase Transition in $Ce_{0.8}La_{0.1}Th_{0.1}$

Singleton, J., NHMFL/LANL
Harrison, N., NHMFL/LANL
Lashley, J.C., NHMFL/LANL
Mielke, C.H., NHMFL/LANL
Drymiotis, F., NHMFL/LANL
Fisk, Z., NHMFL

The γ-α structural phase transition in the (Ce,Th,La) system has attracted considerable attention (see e.g., Ref. 1 and references therein). As part of a project on electronically-driven phase transitions in Pu and other systems, we have studied $Ce_{0.8}La_{0.1}Th_{0.1}$ using multiturn compensated magnetometers in pulsed fields of up to 60 T. As the γ-α transition involves thermal relaxation over an extended period of time, the experiments required the establishment of a rigorous thermal-cycling protocol before each field sweep to ensure reproducibility.

It is possible to identify behavior characteristic of each phase in their magnetization (M) vs. magnetic field strength (H) relationships (Fig. 1).[2] At very low temperatures, the α phase shows an M vs. H curve with a smaller gradient than that of the γ phase ($T > 47$ K). In the intermediate temperature regime, a transition between the two types of behavior can be seen as an elbow in the M vs. H curves (Fig. 1). The transition is more prominent in susceptibility (dM/dH) data, and its position can be mapped onto a temperature-field

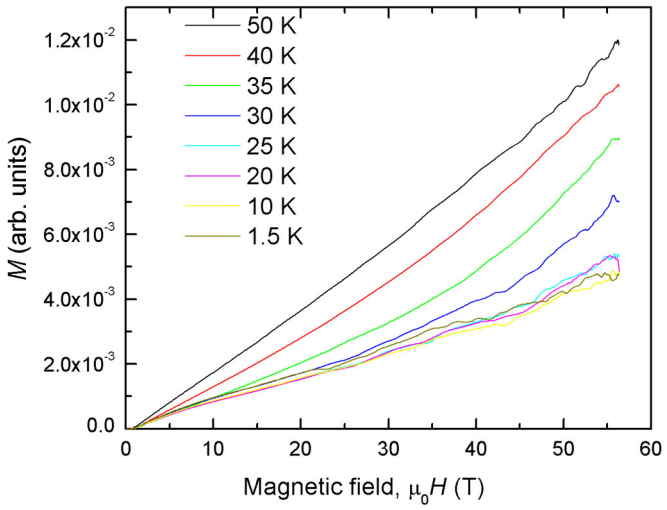

Figure 1. Selected magnetization (M) vs. applied field (H) data for $Ce_{0.8}La_{0.1}Th_{0.1}$ at various temperatures. Note the limiting behavior at high and low temperatures; at intermediate temperatures, an "elbow" can be seen, indicating a transition between the two types of behavior.

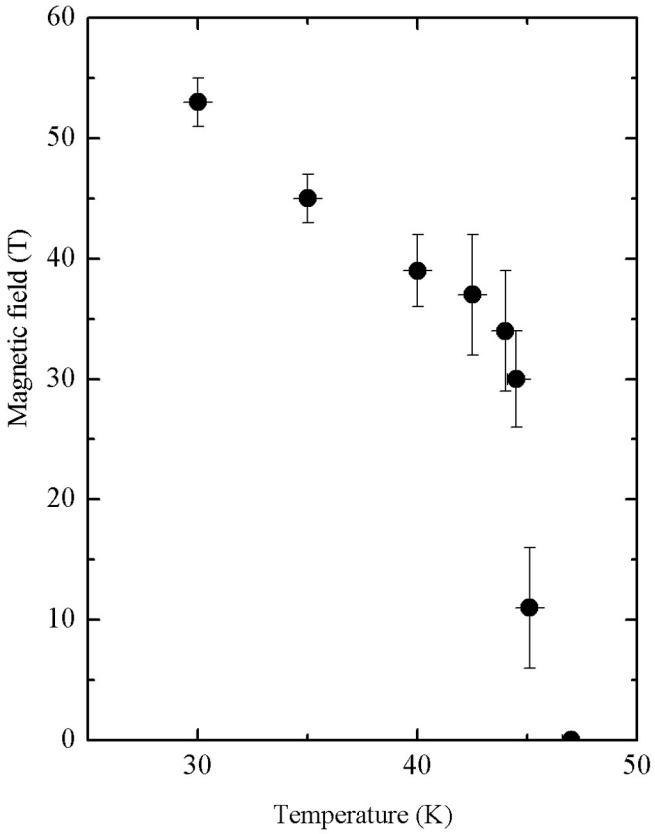

Figure 2. Field vs. temperature phase diagram showing the position of the "elbow" in the M vs. H curves.

phase diagram (Fig. 2); it extrapolates to a zero-field limit which corresponds to the known γ-α transition temperature (47 K).[2] A series of contactless conductivity measurements have also been performed on the compound to pulsed magnetic fields to 60 T. The conductivity (as determined by the skin depth) shows a significant change in conductivity (break in slope) as a function of magnetic field. The temperature dependence of the feature in σ(H,T) is consistent with that of the dM/dH data.

It is appealing to link the transition seen in the magnetization to the γ-α phase boundary; if this is the case, it represents a new member of the rare class of structural phase transitions that it is possible to tune using applied magnetic field. On the other hand, the elbow in the M vs. H curves may be the precursor to a metamagnetic transition. Further experiments to test these hypotheses are in progress.

Acknowledgements: This work was supported by U.S. Department of Energy grant LDRD-DR 20030084.

[1] Thompson, J.D., *et al.*, *Phys. Rev. Lett.*, **50**, 1081-1084 (1983).
[2] Singleton, J., *et al.*, preprint.

Commissioning Experience on 65 T Gap Cooled Prototype Magnets

Swenson, C.A., NHMFL
Marshall, W.S., NHMFL
Gavrilin, A.V., NHMFL
Miller, E.L., NHMFL
Ruminer, P.F., NHMFL/LANL
Rickel, D., NHMFL/LANL

A new 65 T short pulse user magnet is now in operation at the NHMFL pulsed field scientific facility. The measured performance specifications are:

- 65 T maximum scientific user field **(8% increase)**
- 3.1 ms in pulse width at 98% B_{max} **(100% increase)**
- 20-25 min shot to shot cool-down time **(~50% reduction).**

The new design incorporates several novel features enhancing performance and coil reliability. The magnet is a nested cylindrically symmetric two-coil assembly in which the inner "A" coil is mechanically isolated from the outer "B" coil. The assembly incorporates a large annular gap in the region separating the two coils. The gap region functions as cooling manifold that is coupled to the surrounding liquid nitrogen bath. The construction of the inner "A" coil is also novel as it introduces a poly-layer assembly technique. The poly-layer assembly technique has been developed for the 100 T insert program to enhance reliability. The inner "A" coil assembly has internal layer to layer interconnections rather than continuous conductor transitions. Fig. 1 presents a cutaway view of the 65 T assembly, which has many other novel features. Fig. 2 presents a comparison of pulsed field waveforms illustrating the improvements achieved with this system.

Prototype testing began in June 2003. We experienced, in prototype #1, a soft failure mode in the outer monolithic coil of the 65 T. Several theoretical mechanisms were developed to explain the behavior of the outer coil. Modifications were made to the prototype #2 assembly to evaluate these engineering hypotheses. The second prototype assembly was tested in July 2003. A soft failure was also observed confirming an insulation breakdown model on the bore of the outer coil. The outer coil assembly was completely redesigned in August 2003. We accomplished the following: (1) developed and implemented a new insulation configuration on the inner bore conductor, (2) developed a toughened epoxy system for the wet lay-up windings, (3) developed an entirely new layer to layer transition geometry, (4) redesigned the outer support shell to limit conductor strain, and (5) implemented the design changes in prototype construction.

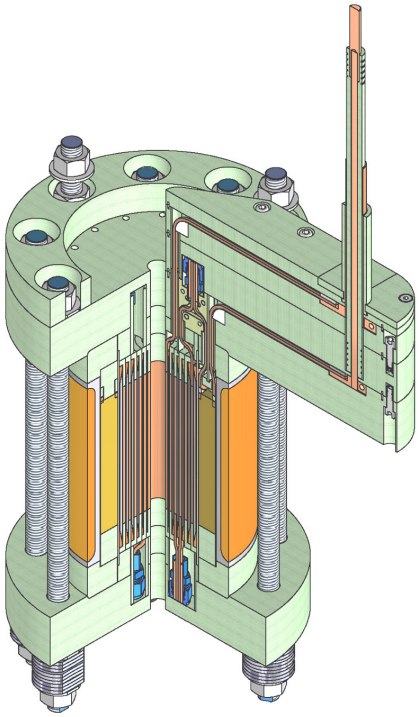

Figure 1. Cutaway view of 65 T magnet assemblies illustrating the two coil nested coil geometry and coaxial lead structure.

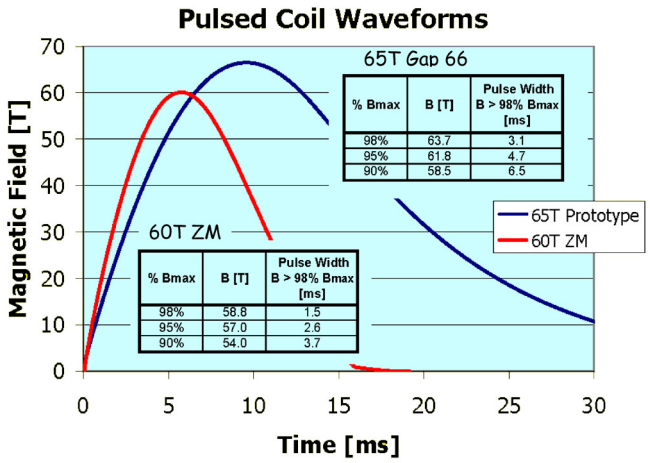

Figure 2. Pulsed field waveform comparison between 65 T gap cooled magnets and 60 T ZM series user magnets.

The third "B" coil assembly was fabricated in September 2003. Prototype #3 performance testing started in October 2003; it passed its testing protocol and is now in user operation. Prototype #3 is now transitioning into operational use as a high field research magnet. The prototype #3 magnet assembly has, as of March 2004, accumulated: 12 shots > 66 T, 56 shots at 65 T, and 240 shots at 63 T. A second "redesigned" 65 T magnet assembly, designated prototype #4, was shipped to the user facility in December 2003. Production of this design series will continue in 2004. We are now operating reliable high-field magnet assemblies at the 1.3 MJ energy level. This is a significant step toward NHMFL development of higher field scientific magnets for the user facility.

A New Representation for MQMAS NMR [IHRP]

Gan, Z., NHMFL
Kwak, H., NHMFL
Alam, T.M., Sandia National Laboratories
Vold, R., College of William and Mary, Applied Science
Hoatson, G., College of William and Mary, Physics

Two-dimensional (2D) MQMAS and STMAS NMR experiments have become widely used for removing second-order quadrupolar broadening.[1,2] The correlation of multiple-quantum or satellite transitions with the central transition of quadrupolar nuclei yields tilted, ridge-shaped peaks in the 2D spectra. Isotropic spectra can be obtained by a spectral shearing along the indirect dimension. In this report, we propose a new representation that has several advantages over the convention *isotropic* shearing.

The new representation shears 2D MQMAS and STMAS spectra along the indirect dimension by the ratio of the quantum numbers between the two dimensions, 3 for triple-quantum (3Q) MAS, 1 for STMAS and 2 for double-quantum (DQ) STMAS. Such a shearing transformation eliminates the chemical shift along the F_1 dimension leaving only the second-order quadrupolar shift (we name this a *Q*-shearing transformation). The resulting 2D spectra require a much smaller F_1 spectral window covering only the second-order quadrupolar width. The small window allows for rotor-synchronization and reduced numbers of t_1-time increments of the 2D experiments. Fig. 1 shows a comparison of ^{93}Nb MQMAS spectra obtained using the *isotropic* and the *Q*-shearing transformation. The *isotropic*-sheared spectrum (Fig. 1a) has spinning sidebands along both dimensions being repeatedly folded due to the small F_1 spectral window set by the spinning frequency and the large chemical shift anisotropy. The *Q*-sheared spectrum (Fig. 1b) has all the spinning sidebands aligned along the F_2 direction (I-axis). A large spectral window can be easily set along the direct detected dimension, and a rotor-synchronized window along F_1 (Q-axis) is sufficient to cover the second-order quadrupolar shift. Isotropic-sheared spectra can be obtained by an additional second shearing along F_2. The final Q-sheared spectra display the isotropic shift and their spinning sidebands along one direction and only the second-order quadrupolar shift along the other spectral direction (Q-axis).

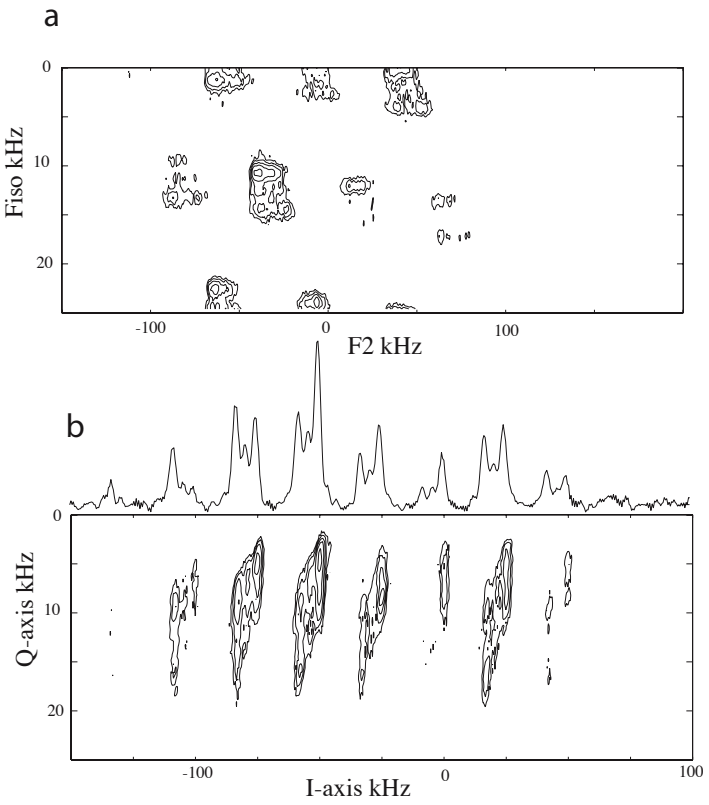

Figure 1. ^{93}Nb MQMAS spectra of the dodecaniobate Keggin material, $Na_{16}[SiNb_{12}O_{40}]\bullet 4H_2O$ obtained with (a) the conventional isotropic-shearing and (b) the proposed *Q*-shearing transformation. The NMR spectra were acquired at 19.6 T with 25 kHz MAS frequency.

The new shearing method avoids the spectral window problem of MQMAS and STMAS experiment and presents the spectra in a clear way. It is particularly useful at high magnetic fields because the old presentation requires a very large spectral window to cover the field-proportioned MQ chemical shift where as the new representation needs only a small spectral window to cover the second-order quadrupolar shift (which are reduced by the high fields).

Acknowledgements: This research was supported by the NHMFL IHRP. Sandia (TMA) is a multiprogram laboratory operated by Sandia Corporation, a Lockheed Martin Company, for the U.S. Department of Energy's National Nuclear Security Administration under Contract DE-AC04-94AL85000.

[1] Frydman, L., *et al.*, *J. Am. Chem. Soc.* **117**, 5367-5368 (1995).
[2] Gan, Z.H., *J. Am. Chem. Soc.* **122,** 3242-3243 (2000).

de Haas – van Alphen Oscillations in $SrRuO_3$

Alexander, C.S., NHMFL
McCall, S., NHMFL
Zhou, Z.X., NHMFL
Zhang, X.H., NHMFL
Purcell, K., NHMFL
Crow, J.E., NHMFL
Cao, G., Univ. of Kentucky, Physics and Astronomy

$SrRuO_3$ has been studied for more than 40 years, but a detailed understanding of the electronic structure in this system has remained elusive. Theoretical predictions of the electronic band structure have not been fully tested by experiments.[1] Verifying these predictions requires experimental data describing the Fermi surface. Previous work was limited to thin film samples, which allowed only a limited range of angular orientations to be studied.[2] Only recently have single crystal samples of sufficiently high quality become available to allow the observation of quantum oscillations in the resistivity and magnetization. This report summarizes the results of experiments recently conducted at the NHMFL millikelvin facility utilizing an Oxford Instruments 18 T superconducting magnet with a dilution refrigerator to measure de Haas – van Alphen oscillations in the magnetization.

The single crystal samples used in this study were carefully characterized prior to measurement. To be certain that the samples used were not crystallographically twinned, they were initially examined using differential interference contrast optical polarized light microscopy and Laue X-ray diffraction and later subjected to TEM analysis. The samples were checked for purity and phase integrity by measuring the zero field resistivity and magnetic susceptibility. The samples used in this study have a residual resistivity ratio (RRR = R(300 K)/R(4 K)) of 140, which is an order of magnitude better than any previous samples.

Magnetization was measured with a phosphor bronze cantilever magnetometer. Due to the large magnetic moment below T_C = 165 K, the cantilever stiffness had to be carefully adjusted to provide sufficient sensitivity without saturating. The magnetization was measured as a function of applied field for several orientations of the crystal. The sample was rotated between H || ab-plane (0 degrees) and H || c-axis (90 degrees) in five degree increments. Typical results are shown in Fig. 1a. The background magnetization was subtracted using a low order polynomial fit to the data and the resulting oscillations were analyzed with a standard FFT algorithm to determine the frequencies of the oscillations

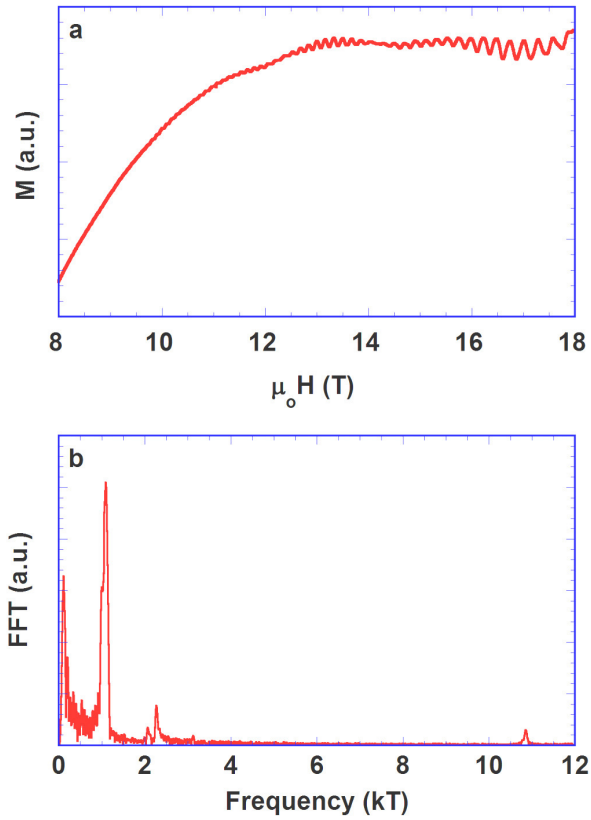

Figure 1. Magnetization data (a) taken at 30 mK with the applied field 70 degrees from the ab-plane. The resulting frequency spectrum (b) after FFT analysis of the oscillations shows several fundamental frequencies ranging between 100 and 11,000 T.

present. The resulting spectrum is shown in Fig. 1b. At least seven fundamental frequencies of oscillation are observed ranging between 100 and 11,000 T. There is a possible indication of one additional frequency at 30 T. Accurately resolving frequencies this low, however, requires that magnetization measurements be made over a larger field range than was accessible in this magnet. Band structure calculations predict nine fundamental frequencies existing in this material.

The temperature dependence of the oscillation amplitude was studied between 30 mK and 650 mK. From these results the electronic effective mass is estimated to range between 2.83 and 6.22 electron masses for the frequencies detected. This range is consistent with the theoretical prediction of 3.7 electron masses.

This work will be very useful in determining the validity of existing theoretical models of the band structure of $SrRuO_3$. Further study of this material, to include a greater number of crystal orientations, will lead to a complete experimental determination of the Fermi surface and ultimately will serve as the basis for understanding the electronic properties of this material.

[1] Mazin, I.I., *et al.*, *Phys. Rev. B*, **56**, 2556 (1997).
[2] Mackenzie, A.P., *et al.*, *Phys. Rev. B*, **58**, R13318 (1998).

3 Omega Thermal Conductivity Measurement of $Nd_{0.5}Sr_{0.5}MnO_3$

Kim, D., NHMFL/LANL
Kim, K-H., NHMFL/LANL
Betts, J.B., NHMFL/LANL
Balakirev, F., NHMFL/LANL
Sohn, J.Y., NHMFL/LANL
Migliori, A., NHMFL/LANL
Lee, J., LANL/STC
Jia, Q., LANL/STC
Moritomo, Y., CIRSE, Nagoya Univ., Applied Physics

We developed the 3 omega thermal conductivity measurement technique, an AC technique compatible with pulsed magnetic fields. The thermal conductivity of a single crystal $Nd_{0.5}Sr_{0.5}MnO_3$ was measured in static magnetic fields.[1] The sample has 2 phase transitions; a ferromagnetic phase transition near 260 K and an antiferromagnetic/charge ordering phase transition near 170 K. The FM transition is thought to be second order and the thermal conductivity increases at the FM region because of the increased electron and phonon contributions. On the other hand, the AFM/CO transition is first order according to the observed hysteresis. The thermal conductivity at the AFM/CO drastically decreases because of the decreased electron and phonon contributions. Also T_N is decreased by applying magnetic field, because the FM state becomes favorable. Applying a high magnetic field over 7 T eventually wipes out AFM/CO state. The thermal conductivity measurement agrees well with the electrical resistivity measurement.[2]

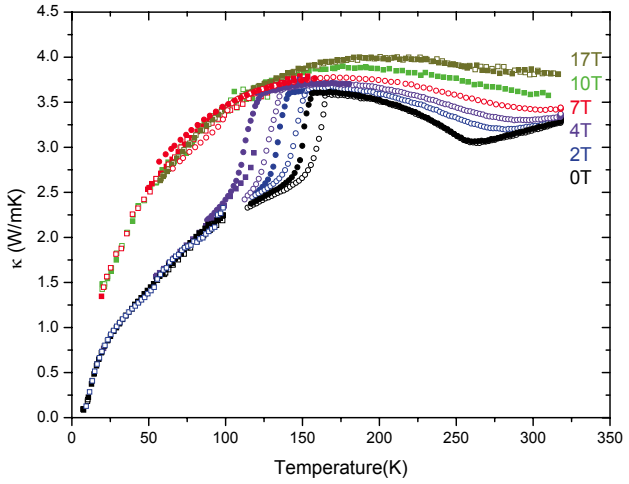

Figure 1. Thermal conductivity of $Nd_{0.5}Sr_{0.5}MnO_3$. Filled symbols: data taken with decreasing temperature. Unfilled symbols: data taken with increasing temperature.

Acknowledgements: This research was performed under the auspices of the NSF, the State of Florida, and DOE.

[1] Kim, D., *et al.*, paper in preparation.
[2] Tokura, Y., *et al.*, *PRL*, **76**, 3164 (1996).

Glassy Behavior of Electrons Near Metal-Insulator Transitions

Dobrosavljević, V., NHMFL
Tanasković, D., NHMFL
Pastor, A.A., NHMFL

Understanding the metal-insulator transition (MIT) poses one of the most basic questions of condensed matter science. The interplay of the electron-electron interactions and disorder is particularly evident deep on the insulating side of the metal-insulator transition (MIT). Here, both experimental and theoretical studies have demonstrated that they can lead to the formation of a soft "Coulomb gap," a phenomenon that is believed to be related to the glassy behavior of the electrons. Such glassy freezing has long been suspected to be of importance, but very recent experiments[1] have suggested that it may even dominate the MIT behavior in certain low carrier density systems.

Theoretically, the possibility for glassy behavior in the charge sector had been anticipated a long time ago in situations where the electrons are strongly localized due to disorder. For well delocalized electronic wave functions, one expects a single well defined ground state and absence of glassiness. At present, little is known as to the precise role and stability of the glassy phase close to the metal-insulator transition (MIT). On physical grounds, one

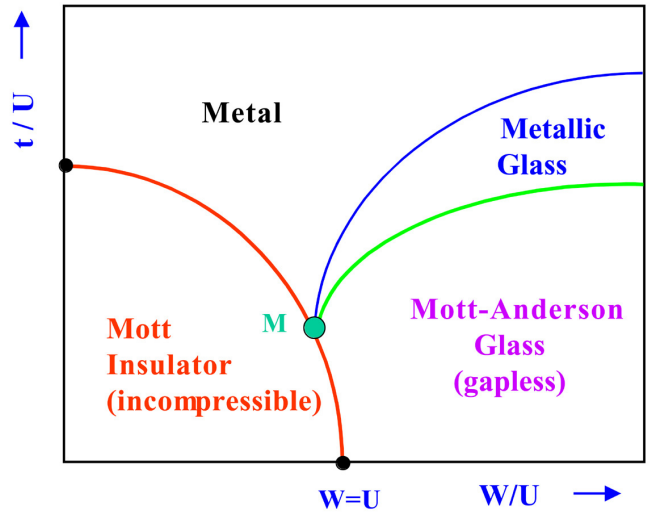

Figure 1. Global phase diagram for the disordered Hubbard model, as a function of the hopping element *t* and the disordered strength *W*, both expressed in units of the on-site interaction *U*. The size of the metallic glass phase is determined by the strength of the inter-site interaction *V*.

expects the quantum fluctuations associated with mobile electrons to suppress glassy ordering, but their precise effects remain to be elucidated. Note that even the *amplitude* of such quantum fluctuations must be a singular function of the distance to the MIT, since they are dynamically determined by processes that control the electronic mobility.

To clarify the situation, we have carried out theoretical studies[2] in order to address the following physical questions: (i) Does the MIT coincide with the onset of glassy behavior? (ii) How do different physical processes that can localize electrons affect the stability of the glassy phase? Our results have provided simple and physically transparent answers to both questions. We find that (a) glassy behavior generally emerges before the electrons localize; (b) Anderson localization enhances the stability of the glassy phase, while Mott localization tends to suppress it. The resulting theoretical phase diagram[2] is shown in the Fig. 1. Our predictions have been confirmed by recent experiments,[1] which have been carried out using high-field facilities at the NHMFL.

Acknowledgements: This work was supported by the NSF grant DMR-9974311.

[1] Bogdanovich, S., *et al.*, *Phys. Rev. Lett.*, **88**, 236401 (2002); Jaroszynski, J., *et al.*, *Phys. Rev. Lett.*, **89**, 276401 (2002).
[2] Dobrosavljević, V., *et al.*, *Phys. Rev. Lett.*, **90**, 016402 (2003).

Probing the Fermi Surfaces of Quasi-Two-Dimensional Organic Superconductors by High Field Resonant Microwave Conductivity Techniques

Takahashi, S., UF, Physics
Petukhov, K., UF, Physics
Kovalev, A.E., UF, Physics
Benjamin, D., UF, Physics
Hill, S., UF, Physics/NHMFL
Qualls, J.S., Univ. of Texas Pan American, Physics and Geology
Kawano, K., Toho Univ., Chemistry and Physics (Japan)
Tamura, M., Toho Univ., Chemistry and Physics
Naito, T., Hokkaido Univ., Graduate School of Science, Chemistry (Japan)
Kobayashi, H., Institute of Molecular Science (Japan)

Similar to the high-T_c superconductors (HTSC), the κ-$(ET)_2X$ [X = $Cu(NSC)_2$ and I_3; ET is short for bis-ethylenedithio-tetrathiafulvalene] organic charge-transfer-salts have quasi-two-dimensional electronic properties and a superconducting ground state, with T_c = 10.4 and 3.6 K, respectively. The κ-$(ET)_2X$ salts also have a similar phase diagram to the HTSC in which an insulating antiferromagnetic phase and conventional and unconventional metallic phases coexist. The precise nature of the superconductivity of κ-$(ET)_2X$ is still uncertain, but the topology of the Fermi surface (FS), especially its nesting characteristics,

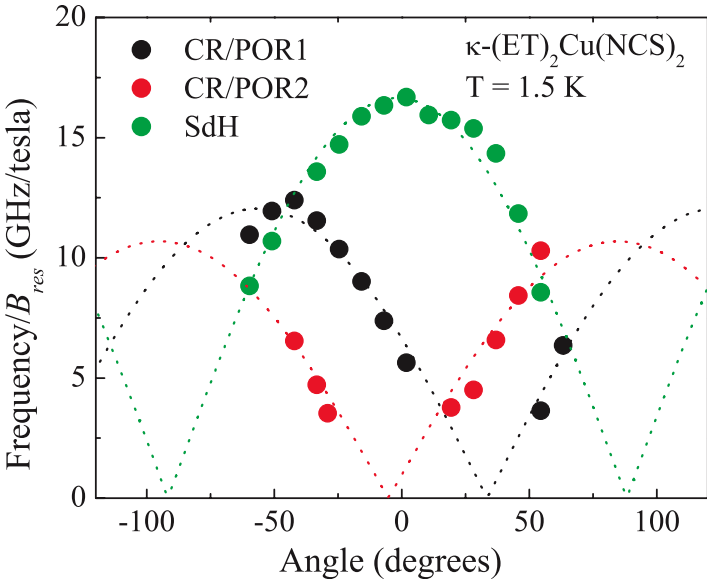

Figure 1. The angle dependence of the CR for κ-$(ET)_2Cu(NSC)_2$. The data were obtained for a single rotation plane containing the normal to the conducting layers; θ is measured relative to this direction.

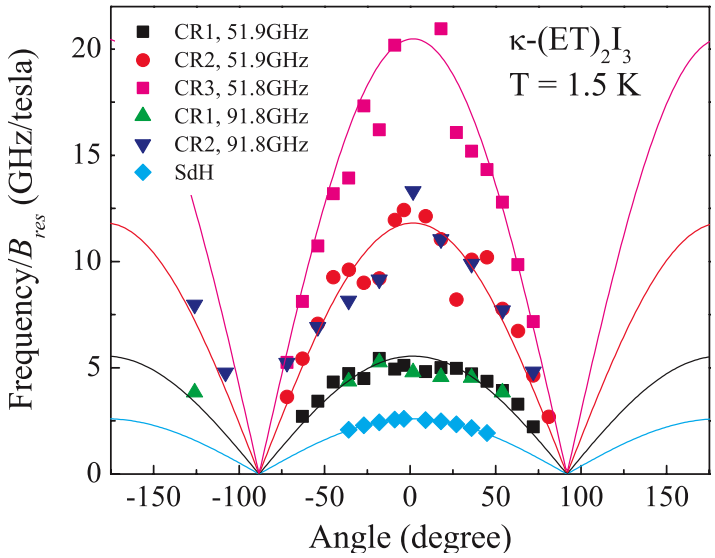

Figure 2. The angle dependence of the CR for κ-$(ET)_2I_3$. The data were obtained for a single rotation plane containing the normal to the conducting layers; θ is measured relative to this direction.

appears to be important.[1] In this report, we briefly discuss preliminary FS measurements for κ-$(ET)_2Cu(NSC)_2$ and κ-$(ET)_2I_3$, which we probe using a novel high-frequency (microwave) angle-dependent magnetoresistance technique.[2]

For both κ-$(ET)_2X$ salts, measurements were conducted using a novel rotating microwave cavity (described in a separate report) which fits into the 33 T resistive magnets at Tallahassee. For a typical field sweep, a series of cyclotron-resonance-like (CR) absorptions are observed in the microwave conductivity. The origins of these resonances depend on the precise topology of the FS, and have been discussed in several earlier publications.[2-4] Fig. 1 shows the angle dependence of the positions of resonant peaks (B_{res}), divided by frequency, for a single rotation plane for κ-$(ET)_2Cu(NSC)_2$ (θ measures the angle between the applied field and the normal to the conducting layers); Fig. 2 shows a similar result for κ-$(ET)_2I_3$. Measurements were then repeated for several planes of rotation. By comparing with the angle dependence of Shubnikov-de Haas (SdH) oscillations, which are also seen in the measurements, one sees that behavior of the CR is quite different for these two salts, in spite of the fact that their FSs are quite similar. For the κ-$(ET)_2Cu(NSC)_2$ salt, the CR are dominated by open FS sheets, whereas the data for κ-$(ET)_2I_3$ is dominated by closed orbits. We speculate that this difference is due to magnetic breakdown. Indeed the large effective mass deduced for the κ-$(ET)_2I_3$ salt seems to confirm this conclusion. Further studies are in progress.

Acknowledgements: This work was supported by NSF (DMR0239481 and DMR0196430) and Research Corporation.

[1] Biggs, T., *et al*., *J. Phys.: Condens. Matter,* **14**, 26, L495-L502 (2002).
[2] See e.g., Kovalev, A.E., *et al*., *Phys. Rev. B*, **66**, 134513 (2002).
[3] Hill, S., *Phys. Rev. B*, **55**, 4931 (1997).
[4] Kovalev, A.E., *et al*., *Phys. Rev. Lett*., **91**, 216402 (2003).

Mapping the Fermi Velocity in the Quasi-2D Organic Conductor κ-$(BEDT\text{-}TTF)_2I_3$

Kovalev, A.E., UF, Physics
Hill, S., UF, Physics/NHMFL
Kawano, K., Toho Univ., Chemistry and Physics (Japan)
Tamura, M., Toho Univ., Chemistry and Physics
Naito, T., Hokkaido Univ. Graduate School of Science, Chemistry (Japan)
Kobayashi, H., Institute of Molecular Science, Okazaki (Japan)

We demonstrate a new method for determining the Fermi velocity in quasi-two-dimensional (Q2D) organic conductors.[1] Application of a magnetic field parallel to the conducting layers results in periodic open orbit quasiparticle trajectories along the Q2D Fermi surface (see Fig. 1a). Averaging of this motion over the Fermi surface leads to a resonance in the interlayer microwave conductivity. The resonance frequency ω_c is simply related to the extremal value of the Fermi velocity perpendicular to the applied field [$v_\perp^{ext}(\psi)$]. Thus, angle dependent microwave studies enable a complete mapping of the Fermi velocity. Measurement of ω_c, as a function of the field orientation ψ within the *xy*-plane, yields a polar plot of $v_\perp^{ext}(\psi)$. The procedure for mapping $v_F(\phi)$ is then identical to that of reconstructing the FS of a Q2D conductor from the measured periods of Yamaji oscillations.[1] Analytically, assuming one can measure $v_\perp^{ext}(\psi)$, it is possible to generate the Fermi velocity $v_F(\phi)$ using the following transformations (see also Fig. 1b):

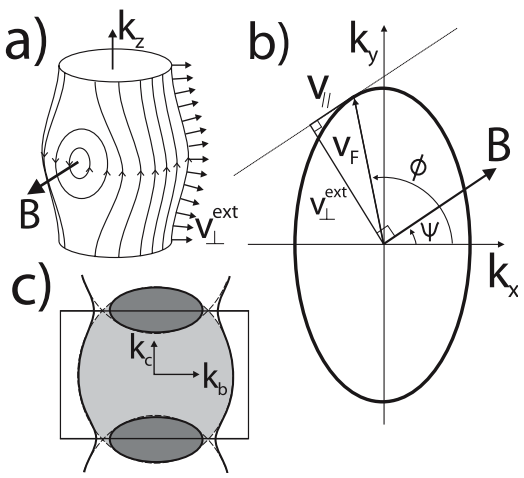

Figure 1. (a) An illustration of the quasiparticle trajectories on a warped Q2D FS cylinder for a field oriented perpendicular to the cylinder axis. The resulting trajectories lead to a weak modulation of the quasiparticle velocities parallel to k_z and, hence, to a resonance in σ_{zz}. (b) The thick line shows $v_F(\phi)$ according to Eq. 1; the right angle triangle illustrates the relationship between $v_\perp^{ext}(\psi)$ and $v_F(\phi)$. (c) The Fermi surface of κ-$(BEDT\text{-}TTF)_2I_3$.[1]

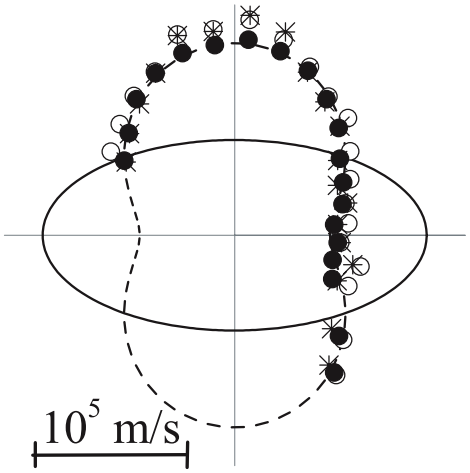

Figure 2. Polar plot of experimentally obtained $v_\perp^{ext}(\psi)$; the dotted line is a fit and the solid line is the resultant $v_F(\phi)$.

$$\nu_F = \sqrt{(\nu_\perp^{ext})^2 + \nu_{||}^2}; \quad \phi = \psi + \arctan\left(\frac{\nu_\perp^{ext}}{\nu_{||}}\right); \quad \nu_{||} = -\frac{d\nu_\perp^{ext}}{d\varphi} \qquad (1)$$

We illustrate the applicability of this method for the highly-2D organic conductor κ-(BEDT-TTF)$_2$I$_3$ in Fig. 2.

Acknowledgements: This work was supported by NSF (DMR0239481 and DMR0196430) and Research Corporation.

[1] Kovalev, A.E., *et al*., *Phys. Rev. Lett*., **91**, 216402 (2003).

OTHER CONDENSED MATTER

Spin Entropy and the Suppression of Thermopower by an In-Plane Field in $Na_{0.71}CoO_2$

Wang, Y., Princeton Univ., Physics
Ong, N.P., Princeton Univ., Physics
Rogado, N.S., Princeton Univ., Physics
Cava, R.J, Princeton Univ., Physics

Thermoelectric cooling and power generation have great advantages over more conventional techniques because they are quieter, more reliable, and environmentally friendly. The search for better thermoelectric materials has been an active area of research. Recently, Na_xCoO_2 has attracted considerable attention because it displays an anomalously large thermopower (***S***) as well as metallic conductivity.[1] To determine the origin of the enhanced thermopower in Na_xCoO_2, we applied a magnetic field along the conducting CoO_2 plane.[2] Since the in-plane field only couples to the spin degrees of freedom, the field dependence of ***S*** will tell us if spin entropy plays an important role in the enhancement of ***S***.

Because a thermopower measurement picks up stray thermoelectric signal from the electrical leads, it is important to calibrate and check for a field dependence in the background signal from the leads. For the leads, we chose phosphor-bronze wire, which is a highly disordered alloy whose field dependence should be small. To measure the absolute value of ***S*** of the wires in a field, we connected a pair of them to the high-T_c superconductor $La_{2-x}Sr_xCuO_4$ (LSCO). In the superconducting state, ***S*** from LSCO should be absolutely zero, so all the signals are from the wires. As shown in the insert of Fig. 1, at low temperatures the phosphor-bronze signal is indeed very small and field independent (the sharp increase marks the vortex solid to liquid transition of LSCO). Thus, all the field dependence of ***S*** in our measurements is really from the samples.

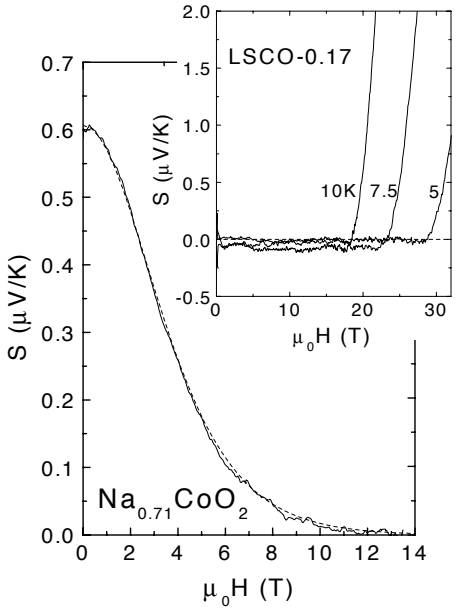

Figure 1. Main panel: The ***S*** vs. *H* curve of Na_xCoO_2 at T = 2.5 K, the broken line is the theoretical fit. Insert: The ***S*** vs. *H* curves of the electrical leads connected to LSCO high T_c superconductors.

As shown in the main panel of Fig. 1, the thermopower of Na_xCoO_2 at low temperatures is strongly suppressed by an in-plane field. At high fields, where the ratio $g\mu_B H/k_B T$ is much larger than 1, ***S*** is suppressed all the way to zero. This behavior is not expected for conventional metals, but is consistent with spin entropy as the origin of the enhanced thermopower in strongly correlated electron systems.[3] In zero field, each spin has 2 possible configurations (up and down) so each electron carries a spin entropy of $k_B$ln2, thus producing a spin thermopower of $k_B$ln2/e = 60μV/K. A magnetic field aligns the spins and reduces the spin entropy. At extremely high field, all spins are aligned along the field direction so the two-fold degeneracy is completely lifted, leading to a vanishing spin thermopower. A simple thermodynamic calculation shows that the field dependence of the spin thermopower should obey the following equation: ***S*** (H,T) / ***S*** $(0,T)$ = {ln[2cosh(u)] –u tanh(u)} / ln2, where $u = g\mu_B H/T$. The broken line in the main panel is the fit using this formula and it agrees very well with the measured curve.

In summary, we have demonstrated experimentally that spin entropy is the likely source of the enhanced thermopower in NaCoO. This suggests that transition metal oxides with strong spin interactions are promising thermoelectric materials.

Acknowledgements: This research is supported by an NSF-MRSEC grant (DMR 0213706), by a contract from the Office of Naval Research (N00014-01-0281), and by a grant from NEDO (Japan). The authors wish to thank Dr. Scott Hannahs for his generous assistance during the experiment.

[1] Terasaki, I., *et al., Phys. Rev. B*, **56**, R12685 (1997).
[2] Wang, Yayu, *et al., Nature*, **423**, 425 (2003).
[3] Chaikin, P.M., *et al*., *Phys Rev. B*, **13**, 647 (1976).

The A_1 and A_2 Transitions in Superfluid ^{3}He in the Presence of Quenched Disorder [IHRP]

Choi, H.C., UF, Physics
Gray, A.J., UF, Physics
Vicente, C.L., UF, Physics/NHMFL
Xia, J.X., UF, Physics/NHMFL
Gervais, G., Northwestern Univ., Physics and Astronomy
Halperin, W.P., Northwestern Univ., Physics and Astronomy
Mulders, N., Univ. of Delaware, Physics and Astronomy
Lee, Y., UF, Physics/NHMFL

Superfluid ^{3}He/Aerogel is the only system in which the effects of quenched disorder on p-wave superfluid can be investigated in a systematic manner. We performed shear impedance measurements on this system (98% porosity aerogel) in the presence of magnetic fields as large as 15 T. The unique geometry of our acoustic cavity allows us to pick up transition signatures from the bulk and liquid in aerogel. We observed the splitting of the superfluid transition into two transitions in high fields both for the bulk ^{3}He and the ^{3}He/Aerogel systems. The field dependence of the splitting in aerogel resembles that of the bulk superfluid ^{3}He, caused by the presence and growth of the A_1 phase. Our results provide the first confirmation of the A_1 phase in superfluid ^{3}He/Aerogel.

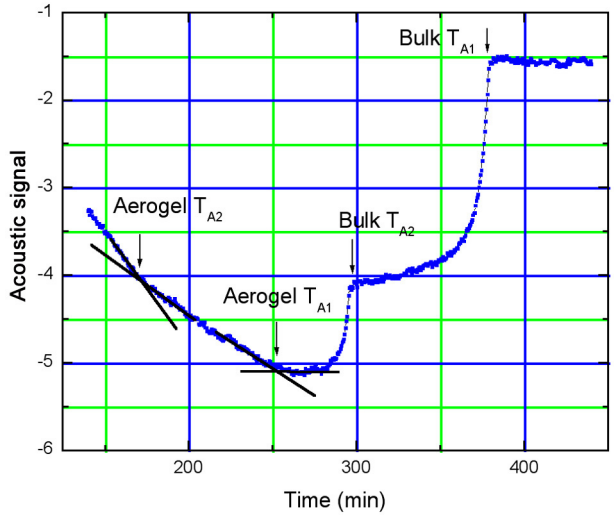

Figure 1. Acoustic impedance measurements taken at B=5 T and P=28.5 bar. The data, taken as the cell is slowly warmed, shows the A_1 and A_2 transitions for ^{3}He both in the bulk and in the aerogel.

Acknowledgements: This work was supported in part by the NSF through DMR-0239483 and IHRP grants.

An AlAs Bilayer System with Interacting 2D Electrons in Different Valleys

Vakili, K., Princeton Univ., Physics
Shkolnikov, Y.P., Princeton Univ., Electrical Engineering
Tutuc, E., Princeton Univ., Physics
De Poortere, E.P., Princeton Univ., Electrical Engineering
Shayegan, M., Princeton Univ., Electrical Engineering

We have characterized a novel AlAs bilayer system, consisting of two parallel quantum wells with different widths. In bulk AlAs, electrons occupy conduction band minima at the X-points of the Brillouin zone. The constant-energy ellipsoids (or valleys) formed at these minima are anisotropic, with a larger conduction mass along the longitudinal direction than along the two transverse directions. This fact, along with the intrinsic strain caused by lattice mismatch with the GaAs substrate on which the wells are grown, causes in-plane valleys to be occupied in wider wells and the out-of-plane valley to be occupied in narrower wells.

For our bilayer system, we grew one wide well (110 Å, in-plane valley) and one narrow well (45 Å, out-of-plane valley) in parallel, separated by a 28 Å GaAs barrier. The sample was mounted on a single-axis rotating stage and magnetotransport measurements

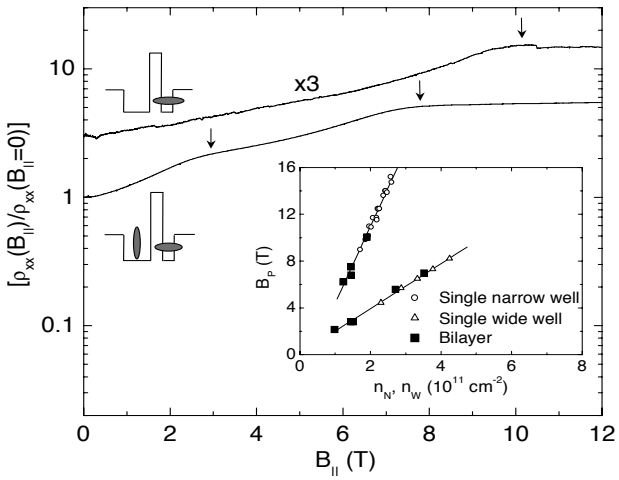

Figure 1. Examples of parallel-field magnetoresistance traces for two different gate voltages, corresponding to different layer densities (n_N=1.9x10^{11} cm^{-2} and n_W=0 for top trace and n_N=n_W=1.5x10^{11} cm^{-2} for bottom trace), with B_P marked by arrows. The inset shows a comparison of the B_P from this sample with those from single quantum well samples.

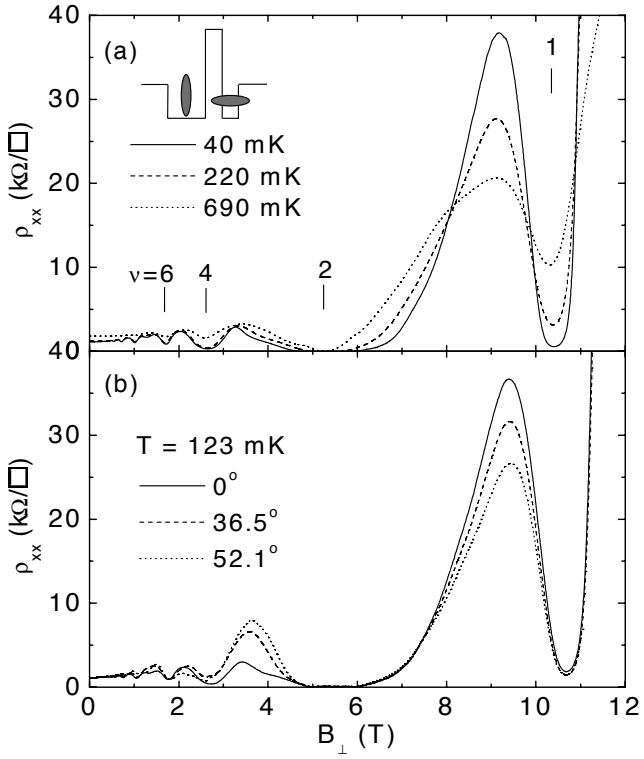

Figure 2. (a) Magnetoresistance in perpendicular field with equal (balanced) charge densities in the two wells (n_N=n_W=1.3x10^{11} cm^{-2}), showing a ν=1 quantum Hall state flanked by a reentrant insulating phase. (b) Angular dependence of the magnetoresistance at balance.

were performed in a dilution refrigerator with magnetic fields up to 18 T. The peak mobility of the sample was 2.2 m^2/Vs, and typical total charge densities were in the range of 2 to 5 x 10^{11} cm^{-2}. We varied the amount of charge in each well with voltages applied to front and back gates and monitored the densities in each well by measuring the different frequency components of low-field Shubnikov-de Haas oscillations.

To demonstrate that different valleys were indeed occupied in each layer, we measured the parallel field magnetoresistance at different gate voltages (Fig. 1) and compared the corresponding spin depopulation fields (B_p) with those measured in single wide and narrow AlAs quantum wells (inset). With equal charge densities in the two wells, we observe a many-body quantum Hall state at total filling factor ν=1 flanked by a re-entrant insulating phase. Despite the small interlayer spacing, our measurements indicate very little tunneling between the layers. For example, there are no odd-integer quantum Hall minima for ν>2 (Fig. 2(a)) and no significant changes in the ν=1 state with applied parallel field (Fig. 2(b)). Thus, we have a clear demonstration of an interacting state of electrons that occupy different conduction band valleys.

Acknowledgements: This work was supported by the NSF. We thank Eric Palm, Tim Murphy, and Glover Jones for technical help.

Development of a $Bi_2Sr_2CaCu_2O_{8+\delta}$ Superconducting Insert Generating 5 T for a Combined Field of 25 T

Weijers, H.W., NHMFL
Trociewitz, U.P., NHMFL
Trociewitz, B., NHMFL
De Jager, A.F., NHMFL
Hascicek, Y.S., NHMFL
Arda, L., NHMFL
Marken, K., Oxford Instruments, Superconducting Technology
Meinesz, M., Oxford Instruments, Superconducting Technology
Miao, H., Oxford Instruments, Superconducting Technology
Hong, S., Oxford Instruments, Superconducting Technology
Schwartz, J., NHMFL/FAMU-FSU College of Engineering

A 25 T magnetic field was generated using a 5 T superconducting $Bi_2Sr_2CaCu_2O_{8+\delta}$ (Bi2212) insert magnet within a 20 T resistive magnet. This insert coil represents a significant step towards 25 T superconducting research magnets and NMR magnets, as this is the first time a superconducting magnet has been operated in a central field of 25 T. Research potentially benefiting from 25 T user magnets covers a wide range of topics in disciplines ranging from physics, materials science and engineering into chemistry and biology.

The insert magnet is constructed using fully reacted powder-in-tube conductor, supplied by Oxford Instruments, Superconducting Technology, Carteret, NJ, and insulated stainless steel reinforcement. The conductor cross-section is 5 mm wide, 0.2 mm thick, and contains 19 Bi2212 filaments. Three concentric sections are used to minimize the total stress in the Bi2212 conductor; two double-pancake stacks and an outer layer-wound section. All sections are constructed using the react-and-wind approach. All sections are electrically connected in series. The insert magnet operates at 4.2 K in a 0.168 m diameter cryostat fitted to the resistive magnet. The diameter of the free bore of the innermost section is 38 mm, representing a sufficiently large bore to support research usage, Fig. 1.

Prior to coil assembly, every double pancake unit and the layer wound coil was tested at 4.2 K, self-field. In addition, several

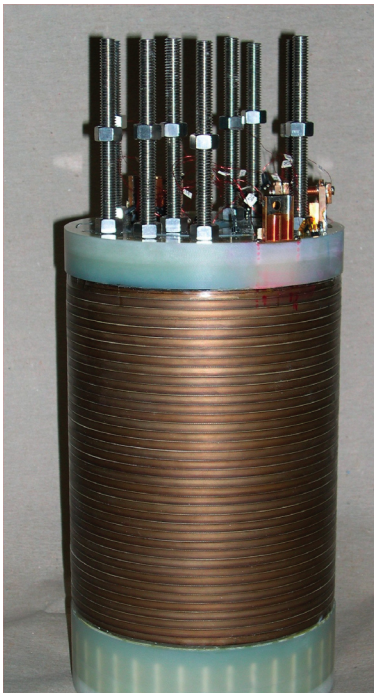

Figure 1. Photograph and schematic cross-section of the Bi2212 insert coil.

double pancake units and a layer-wound coil of half the thickness as the one used in the insert were selected for characterization in high background magnetic field to verify stress tolerance and field dependence of I_c.

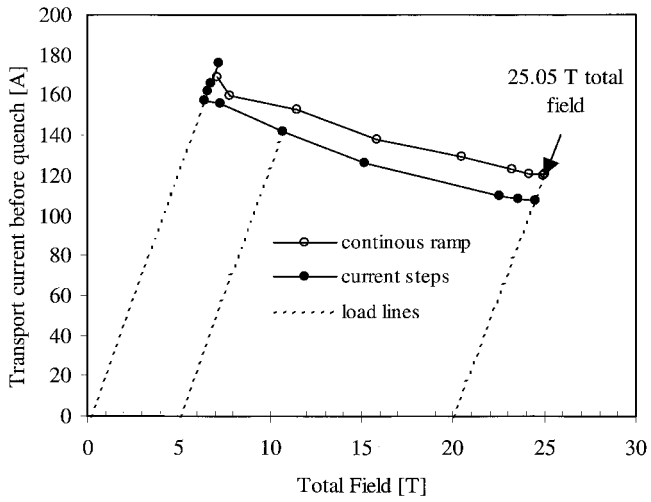

Figure 2. Bi2212 insert coil current before quenching vs. the central magnetic field (LBRM plus insert coil). Some of the HTS insert coil load lines are included to differentiate the contributions of the background magnetic field and the insert coil.

The assembled Bi2212 insert magnet was instrumented with multiple voltage taps, including one across each section. Strain gauges monitored radial and axial strain in the magnet. A Hall effect sensor was placed at center field. A step-and-hold approach was applied for testing the insert coil in self-field and successive background fields of 1, 5, 10, 18, 19, and 19.94 T. In all cases, a thermal runaway, initiated in the innermost section, occurred before the 1 μV/cm criterion was reached in any section of the insert coil. Fig. 2 presents the highest current values before thermal runaway occurred. Changing the measurement procedure from current step-and-hold to constant current ramp rate resulted in higher quench currents. Applying a 3.7 A/s ramp rate for the insert in a 19.94 T background magnetic field results in a quench for an insert current just above 120.4 A. This corresponds to a central field of 25.05 T. The highest stress and strain occurred with the insert and outsert combined to generate 25.05 T and a current of 120.4 A in the insert. Reproducibility of the quench current indicated that the strain in the insert was everywhere below the critical strain and the reinforcement was adequate.[1-4]

[1] Weijers, H.W., *et al.*, *IEEE Trans. on Appl. Supercond.*, **13**, 1396-1399 (2003).
[2] Ohkura, K., *et al.*, *Appl. Phys. Lett.*, **67**, 1923-1925 (1995).
[3] Okada, M., *et al.*, *Adv. in Superconductivity XI*, 851-854 (1999).
[4] Weijers, H.W., *et al.*, *Supercond. Sci. Technol.*, **16**, 1-10 (2003).

Hall-Density Anomaly in the Ground State of a High-Temperature Superconductor

Balakirev, F.F., NHMFL/LANL
Betts, J.B., NHMFL/LANL
Migliori, A., NHMFL/LANL
Ono, S., Central Research Institute of Electric Power Industry (Japan)
Ando, Y., Central Research Institute of Electric Power Industry
Boebinger, G.S., NHMFL/LANL

After almost two decades since the discovery of high-temperature superconductors, the mechanism of high temperature superconductivity, whose origin remains a central controversy in condensed matter physics, is not yet established. Many believe that understating the unconventional nature of the normal state of high-temperature superconductors would ultimately lead to understanding the mechanism of high temperature superconductivity. Among the various abnormal normal state properties, the Hall effect has been notoriously difficult to understand.

We report a startling evolution of the low-temperature Hall coefficient in the normal state of the high-temperature superconductor $Bi_2Sr_{2-x}La_xCuO_{6+\delta}$ (BSLCO) as a function of temperature and hole doping, p, by suppressing high-temperature superconductivity with an intense magnetic field.[1] The Hall number per unit cell, $n_{Hall} \equiv V_{cell}/eR_H$, is found to increase rapidly from nearly zero value at the onset of the high-temperature superconducting state (p=0.10) to approximately one hole per unit cell near optimal doping (p=0.16) corresponding to roughly 7 carriers per each hole introduced with doping. At about same hole doping level where superconductivity is most robust, n_{Hall} variation with doping exhibits a sharp change suggesting that two competing ground states underlie the high-temperature superconducting phase.

In marked contrast to behavior seen in high-temperature superconductors at high temperatures, upon cooling R_H becomes relatively temperature independent signaling the recovery of Hall behavior typical of a common metals, thus allowing us to investigate the evolution of the density of states in the low temperature limit. Fig. 1 shows the surprising temperature and doping dependencies of n_{Hall}. We note that the rapid increase of n_{Hall} with doping in the low temperature limit shows a remarkably linear correlation with doping dependence of T_c in the underdoped regime ($p \leq 0.15$) indicating that the superfluid density in the superconducting state corresponds to the carrier density in the underlying normal state throughout the underdoped regime. The

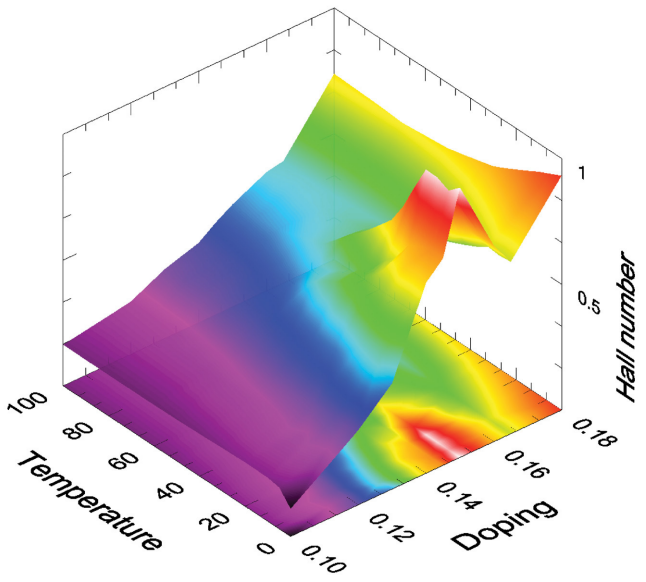

Figure 1. 3D color map plot of the Hall number, $n_{Hall} \equiv V_{cell}/eR_H$, as a function of temperature and doping in $Bi_2Sr_{2-x}La_xCuO_{6+\delta}$. n_{Hall} normalized to give the number of holes per Cu atom. Also shown is the 2D color map projection of the data onto temperature and doping plane. While the high temperature data shows a monotonic evolution of $n_{Hall}(p)$ with increasing doping, upon cooling to ~50 K the anomalous cusp at p=0.15 becomes apparent, which must be associated with an abrupt change in the Fermi surface suggesting a quantum phase transition (QPT) between two different metallic phases in the normal state. This observation also highlights the necessity of the high magnetic fields to reveal the intrinsic normal state behavior at low temperatures.

observed maximum value of n_{Hall} that implies a big Fermi surface that fills close to half a Brillouin zone.

The pronounced cusp in the zero-temperature-limiting value of the Hall number at optimal doping must be associated with an abrupt change in the Fermi surface, and thus suggests a quantum phase transition between two different metallic phases in the normal state of the high-temperature superconductors. From this behavior one can argue that the occurrence of high-temperature superconductivity is fundamentally related to quantum fluctuations associated with a zero-temperature phase transition. Recently a number of models that involve quantum phase transition (QPT) between two different metallic phases in the normal state of the high-temperature superconductors have been the subject of active debate among physicists. It takes an extremely high magnetic field to suppress the superconductivity and reveal a clear signature of a QPT in the normal state in the zero temperature limit.

[1] Balakirev, F.F., *et al.*, *Nature*, **424**, 912 (2003).

National High Magnetic Field Laboratory

1800 East Paul Dirac Drive
Tallahassee, FL 32310-3706
Tel: 850 644-0311
Fax: 850 644-8350
www.magnet.fsu.edu

Non-Profit
Organization
U.S. Postage
PAID
Tallahassee, FL
Permit No. 55

CONFERENCES & WORKSHOPS

2004

Workshop on Solid State NMR and Material Applications at High Magnetic Fields
http://nmr.magnet.fsu.edu/ssnmr_workshop/
March 12-13, 2004
Tallahassee, Florida
Contact: Zhehong Gan (*gan@magnet.fsu.edu*, 850-644-4662)

International Workshop on Materials Analysis & Processing in Magnetic Fields
http://www.magnet.fsu.edu/mat.proc
March 17-19, 2004
Tallahassee, Florida
Contact: Hans Schneider-Muntau (mat.proc@magnet.fsu.edu, 850-644-0863)

Fluctuations and Noise in Materials
http://spie.org/Conferences/Calls/04/fn/conferences/index.cfm?fuseaction=FN03
May 25-28, 2004
Maspalomas, Gran Canaria, Spain
Contact: Dragana Popović (*dragana@magnet.fsu.edu*, 850-644-3913)

16th International Conference on High Magnetic Fields in Semiconductor Physics (SemiMag16)
http://SemiMag16.magnet.fsu.edu
August 2-6, 2004
Abstract Deadline: April 2, 2004
Early Registration Deadline: June 25, 2004
Tallahassee, Florida
Contact: Yong-Jie Wang (*SemiMag16@magnet.fsu.edu*, 850-644-1496)

Applied Superconductivity Conference (ASC04)
http://www.ASCinc.org
October 3-8, 2004
Abstract Deadline: March 15, 2004
Jacksonville, Florida
Contact: Justin Schwartz (*ASC04ConfChair@magnet.fsu.edu*, 850-644-0874)

15th Conference of the International Society of Magnetic Resonance (ISMAR 2004)
http://www.ismar.org/
October 24-29, 2004
Ponte Vedra Beach, Florida (near Jacksonville)
Contact: Tim Cross (*mail@ismar.org*, 850-644-0917)

2005

Physical Phenomena at High Magnetic Fields – V (PPHMF-V)
August 5-9, 2005
Tallahassee, Florida
Contact: Coordinator Alice Hobbs (*aclark@magnet.fsu.edu*, 850-644-3203)

24th Low Temperature Physics Conference (LT-24)
August 10-17, 2005
Orlando, Florida
Contact: Gary Ihas (*ihas@phys.ufl.edu*, 352-392-9244)